


SAMANWAY CHAKRABORTY

# CFD Investigation on Tailplane Ice Protection System

Faculty of Engineering and Applied Sciences
MSc Aerospace Vehicle Design (Aircraft Design)

MSc
Academic Year: 2024 - 2025

Supervisor: Dr. Amir Zare Shahneh
August 2025




Faculty of Engineering and Applied Sciences
MSc Aerospace Vehicle Design (Aircraft Design)

MSc

Academic Year 2024 - 2025

SAMANWAY CHAKRABORTY

# CFD Investigation on Tailplane Ice Protection System

Supervisor: Dr. Amir Zare Shahneh
August 2025

This thesis is submitted in partial fulfilment of the requirements for the degree of MSc

© Cranfield University 2025. All rights reserved. No part of this publication may be reproduced without the written permission of the copyright owner.

# Academic integrity declaration

I declare that:

- The thesis submitted has been written by me alone.
- The thesis submitted has not been previously submitted to this university or any other.
- That all content, including primary and/or secondary data, is true to the best of my knowledge.
- That all quotations and references have been duly acknowledged according to the requirements of academic research.

I understand that to knowingly submit work in violation of the above statement will be considered by examiners as academic misconduct.

# CFD Investigation on Tailplane Ice Protection System

Samanway Chakraborty

## I.ABSTRACT

In this study, the effectiveness of engine exhaust in shielding aircraft tailplanes from ice accretion a known aviation safety hazard is examined. Three sample aircraft which are Gulfstream G280, Airbus A320 and Airbus A380 were used to run Computational Fluid Dynamics (CFD) simulations, considering important parameters such exhaust temperature, plume dispersion, and flying phase. The A320 was evaluated in four operational conditions: take-off, cruise, runway roll, and taxiing. EASA Type Certificate Data Sheets were used to collect engine exhaust data in order to guarantee realistic boundary conditions.

The results clearly show the differences between aircraft types. Since the engines of the A320 and A380 are situated beneath the wings, the exhaust plumes swiftly disperse beneath the tailplane, creating hardly any heating effect. Due to the absence of a tailplane ice prevention system (IPS), these aircraft would have been subject to weight and fuel penalties. The G280, on the other hand, which has engines situated on the rear fuselage, displayed some tailplane heating and plume impingement. An IPS is still necessary since this natural impact was insufficiently powerful at altitude. The distinction reflects aircraft philosophy: business jets place a higher priority on flexibility and safety margins, whereas high-volume airline aircraft are optimized for efficiency.

Overall, the study confirms that exhaust heat alone cannot provide reliable ice protection. Instead, the findings point towards hybrid approaches where limited natural heating could be combined with technologies like electrothermal or bleed-air systems as a more practical way forward for future aircraft.

Keywords: A320, G280, A380, EASA Type Certificate, Tailplane, Ice Protection System, CFD, Exhaust Flow

## II.NOMENCLATURE

| | |
|---|---|
| CFD | Computational Fluid Dynamics |
| IPS | Ice Protection System |
| EMIPS | Electro-mechanical ice protection systems |
| AoA | Angle of Attack |
| LWC | Liquid Water Content |
| $T_\infty$ | Free-stream Temperature |
| $V_\infty$ | Freestream velocity |
| $V_e$ | Nozzle exhaust velocity |
| M | Mach number |
| a | Speed of sound at altitude |
| R | Specific gas constant for air |
| $p_\infty$ | Ambient static pressure |
| $T_e$ | Nozzle exhaust temperature |
| EGT | Exhaust Gas Temperature |
| k | Thermal conductivity |

### A. Greek Symbols

| | |
|---|---|
| $\rho$ | Air Density |
| $\mu$ | Dynamic Viscosity |
| $\gamma$ | Ratio of specific heats |
| $\rho_\infty$ | Ambient density |

## 1.0 Introduction

Tailplane icing is a critical safety issue in aviation since even a modest amount of icing can disturb airflow, decrease lift, add drag, and in adverse situations, induce tailplane stall. Tailplanes are more susceptible since they get less natural heat and airflow compared to wings and hence are more susceptible to icing in cold weather conditions [1]. Ice on an aircraft can undermine stability and control, particularly during sensitive stages such as take-off and landing. To mitigate this, aircraft are fitted with ice protection systems (IPS) that are intended to prevent or shed ice while conforming to airworthiness requirements such as CS-25 [2], [3], [4].

The aerospace field has dedicated rising attention to the assessment of various IPS systems especially when operating in cold weather environments that create the most challenging icing conditions. The exhaust flow fields from engines may function as therm al protection systems, but their effectiveness depends on engine position and exhaust design and flight operational period. The detailed study of these effects becomes possible through CFD which allows heat transfer simulation alongside airflow interaction modelling at a lower cost than physical experiments [5]

The research uses computational fluid dynamics to analyse exhaust-based tailplane ice protection across three representative aircraft and evaluates various flight phases of a single aircraft during cold-day conditions. The study demonstrates exhaust heating effectiveness and its operational boundaries and demonstrates how integration with electrothermal or bleed-air systems can produce better tailplane de-icing and anti-icing results [6].

### 1.1 Background: Tailplane Icing and Stall Risks

Ice buildup on aerodynamic surfaces alters their geometry and interferes with the surrounding airflow, making aircraft icing a severe threat to flight safety. Often with sudden and severe consequences, this disruption reduces lift, increases drag, and impacts stability and control levels [7]. The horizontal tailplane is particularly vulnerable since, unlike the wing, it receives little benefit from engine exhaust heating or high-speed airflow, leaving it susceptible to rapid ice build-up in cold and moist atmospheric conditions (Figure 1.0-1) [8] Although bigger accretions raise the possibility of a tailplane stall, even relatively thin coatings of ice can alter the local camber and pressure distribution across the tailplane. Such a stall manifests as an abrupt nose-down pitching moment that is especially dangerous during take-off and landing, when the aircraft operates at higher lift coefficients and closer to its stability margins (Figure 1.0-2) [9], [10]



**Figure 1.0-1 Ice accumulation along the leading edge of the ATR 42 tailplane.** [8]

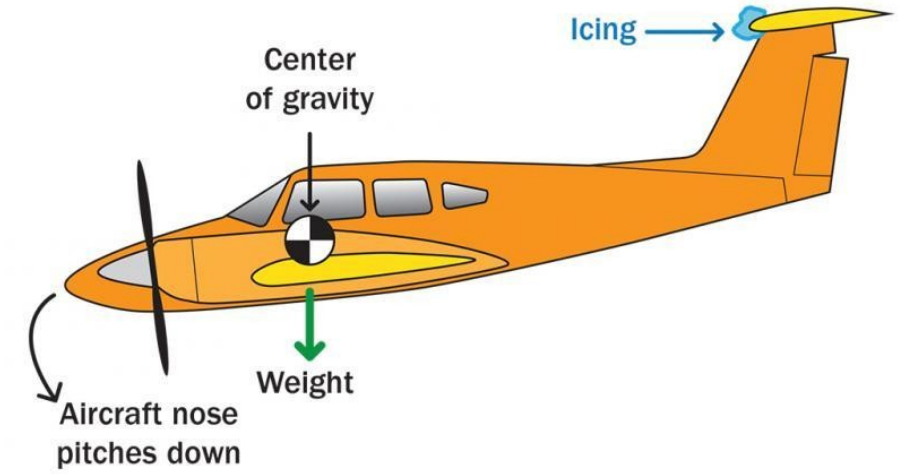



**Figure 1.0-2 Effect of tailplane icing causing nose-down pitching moment** [9]

The overall lift behaviour of contaminated surfaces can be used to highlight the consequences of ice. Compared with a clean configuration, iced airfoil exhibits a lower maximum lift coefficient, a

premature stall angle, and larger separated flow regions, as shown in in Figure 1.0-3 [11] Despite the fact that this picture depicts a wing section, the tailplane follows the same guidelines: Ice development reduces available control power and may reverse the tail's intended stabilizing role by causing flow separation at lower angles of attack. Collectively, Figure 1.0-1, Figure 1.0-2 & Figure 1.0-3 demonstrate the full sequence of effects from ice accumulation to aerodynamic imbalance, to degraded performance emphasizing why effective ice protection systems are essential for maintaining controllability and ensuring safe flight operations under icing conditions.

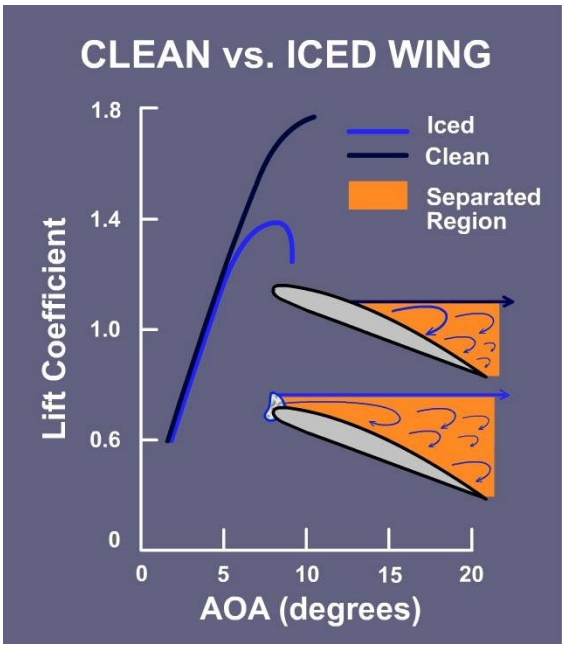



**Figure 1.0-3 Lift reduction in clean wing vs iced wing** [11]

### 1.2 Ice Protection Systems Overview

IPS is utilized either for de-icing, which eliminates produced ice, or anti-icing, which stops ice formation, to stop icing from forming on the aircraft. Several technologies are in use: bleed-air systems, which channel hot compressed air from the engines to leading edges and nacelles electrothermal systems, which apply heat through embedded resistive elements and electro - mechanical ice protection systems (EMIPS), which generate mechanical impulses to fracture and shed ice [12], [13] .

These strategies all have operational trade-offs. Although dependable, bleeding-air systems reduce engine efficiency. The high electrical power needs of electrothermal systems come at the expense of design flexibility and retrofit possibility. Although EMIPS are lighter and more energy-efficient, mechanical durability issues and certification issues prevent them from being widely used [13], [14]. Wings, nacelles, and vital sensors have historically been given priority in IPS development and research, but the tailplane, despite its significance for stability and control, has gotten relatively less attention [12].

Figure 1.0-4 illustrates the ice protection configuration of an Airbus A330. Wing leading edges, engine nacelle inlets, cockpit windows, pitot, static, angle of attack, and temperature probes, and drainage masts are all protected. When there is ice, these systems work together to maintain aerodynamic efficiency and the integrity of critical flight instruments. Notably, there is no indication of specific protection for the tailplane, which is indicative of a trend in the industry where empennage surfaces are not as often given priority for IPS. The need of looking into tailplane icing and creating specialized protection techniques is highlighted by this observation.

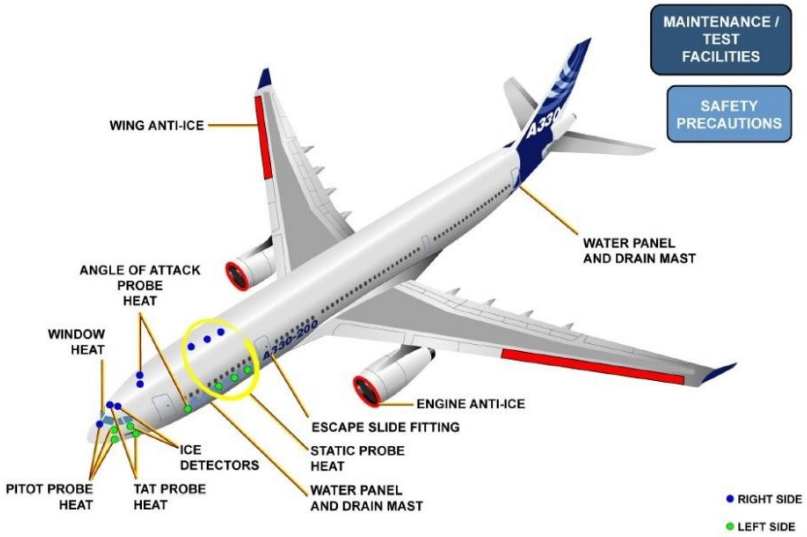



**Figure 1.0-4 A330 ICE PROTECTION SYSTEM** [15]

### 1.3 Research Gaps

Since the aft fuselage region is naturally warmed by the hot jet stream, engine exhaust plumes can offer the tailplane some passive thermal protection. The local thermal environment is shaped by a number of variables, including engine placement, exhaust nozzle design, and flight phase, all of which have a significant impact on how successful this heating is. Because it enables thorough modelling of airflow and heat transfer under ice conditions without the expense and safety concerns of full-scale testing, computational fluid dynamics (CFD) has emerged as a crucial tool for examining these interactions [16], [17]. The majority of CFD research to date has focused on engine nacelles and wings, namely on electrothermal or hybrid methods [17] and hot-air anti-icing systems [16]. The tailplane has received far less attention. Therefore, it is still difficult to determine if exhaust heating alone is sufficient for tailplane protection due to a lack of comparable data across various aircraft layouts and flying phases. Because of this uncertainty, it is unclear if natural exhaust heating is sufficient or if specialized ice protection devices are required to guarantee adherence to airworthiness regulations.

### 1.4 Aim & Objective

The aim of this study is to investigate the interaction between engine exhaust flow fields and the horizontal tailplane in order to assess the extent to which exhaust heating can contribute to ice protection, and to evaluate the potential requirement for a dedicated tailplane ice protection system (IPS).

To achieve this aim, the study first analyses the thermal and velocity distribution of engine exhaust flow fields using both steady-state and transient CFD simulations. It then evaluates the temperature gradients and Mach number in the aft-engine region to determine their effectiveness in providing passive tailplane de-icing. Comparative simulations are performed on three representative aircraft: Airbus A320, Gulfstream G280, and Airbus A380, with the objective of examining the influence of engine installation and exhaust nozzle geometry. In addition, the study investigates the tailplane environment during four operational phases of the A320, namely taxiing, runway roll, take-off, and cruise, under cold-day atmospheric conditions. Realistic thermal and velocity inputs are ensured by applying boundary conditions derived from EASA Type Certificate Data Sheets. Finally, the convergence behaviour of CFD solutions is assessed, and the results are interpreted in the context of a hybrid IPS concept that integrates natural exhaust heating with conventional electrothermal or bleed-air protection strategies.

# 2.0 Literature Review

## 2.1 Aircraft Icing & Safety Risk

A notable example of the limitations of ice protection systems is the accident involving American Eagle Flight 4184, an ATR 72 that crashed near Roselawn, Indiana, in October 1994. The aircraft was fitted with pneumatic de-icing boots on both the wing and tailplane leading edges, but during the flight it entered an area of supercooled large droplet (SLD) icing. These conditions went beyond the certified operating range of the system, allowing ice to build up behind the protected zones. The resulting change in aerodynamic shape caused the aircraft to roll uncontrollably and ultimately led to loss of control. The investigation by the National Transportation Safety Board (NTSB) determined that the IPS operated as designed, but it was not capable of handling the severe icing encountered. This case highlights the vulnerability of conventional IPS when exposed to extreme conditions and demonstrates the continuing safety risks associated with tailplane icing outside certified protection limits [18]



**Figure 2.0-1 The wreckage field from the ATR 72 accident near Roselawn, Indiana**[19]

## 2.2 Ice Protection Systems

Ice buildup on airplane surfaces has long been acknowledged as a major safety risk. Ice protection systems (IPS), which are either intended to prevent ice accretion (anti-icing) or to remove ice once it has formed (de-icing), are installed in airplanes to reduce these dangers. In order to guarantee safe operation during all crucial flight phases, certification criteria demand that IPS be functional within specified icing envelopes [12]

When airplanes come into contact with clouds that contain supercooled water droplets at below-freezing temperatures, icing happens. Larger droplets create glaze ice, which spreads before freezing into dense, transparent layers, whereas smaller droplets usually generate rime ice, which freezes quickly into a rough, opaque deposit [12] Both shapes change airflow and surface geometry, which raises the chance of stalling, decreases lift, and increases drag.

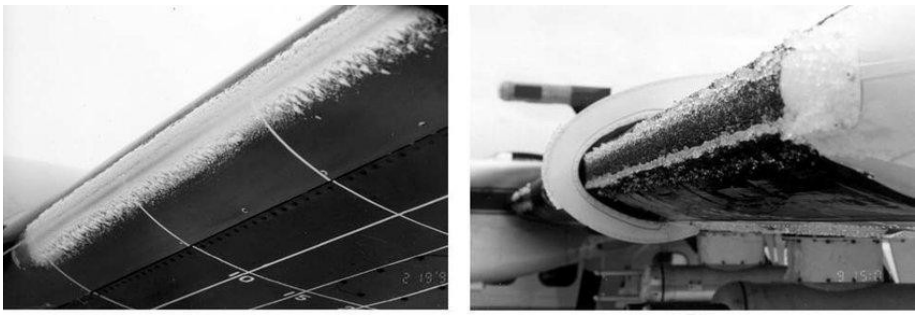


**Figure 2.0-2 Comparison of rime ice (left), formed by small droplets freezing instantly, and glaze ice (right), formed by large droplets freezing slowly** [20]

Lifting surfaces and control surfaces are particularly affected by ice buildup. While wings are the most commonly researched, the horizontal tailplane is also important since ice buildup can cause tailplane stall and hinder pitching moments [21]. This emphasizes how crucial it is to modify IPS for particular aerodynamic conditions.

Appendix C and CS-25.1419, among other certification criteria, state that IPS must function well under both continuous and intermittent ice circumstances. In order to ensure safe operation, systems must safeguard not just wings but also nacelles, propellers, probes, and empennage surfaces.[12] The three main types of IPS technologies are chemical, mechanical, and thermal [13].

*Systems for Protecting Thermal Ice*

By keeping the surface temperature above freezing, thermal systems function. to compressed air from the engine is redirected by bleed-air systems and distributed along the leading edges via piccolo tubes. Although they are dependable, they increase ducting weight and decrease engine efficiency [13]. In order to balance energy utilization, electrothermal systems (ETIPS) insert resistive heaters beneath the surface. These heaters typically run constantly in a parting strip and cyclically elsewhere. Despite their flexibility, they use a lot of electricity [16].

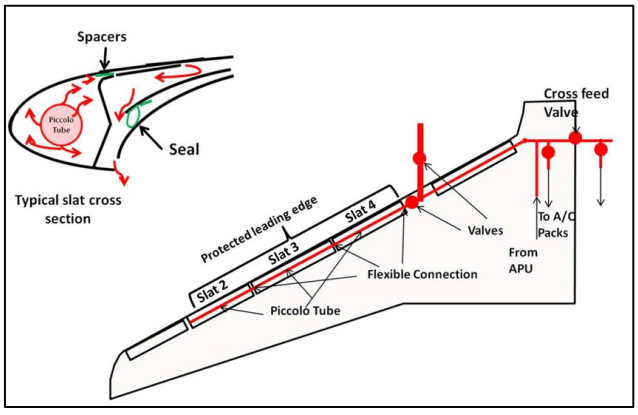



**Figure 2.0-3 Pneumatic and electrothermal wing ice protection systems** [22]

*Systems for Mechanical Ice Protection*

Once produced, ice is broken up or dislodged by mechanical devices. To break the ice, pneumatic boots inflate periodically [13]. Elastomeric actuation or electromagnetic pulses are used in electro-impulse and electro-expulsive systems to shed ice [13]. Though they might not work as well under extreme ice situations, these systems often use less energy than thermal IPS.

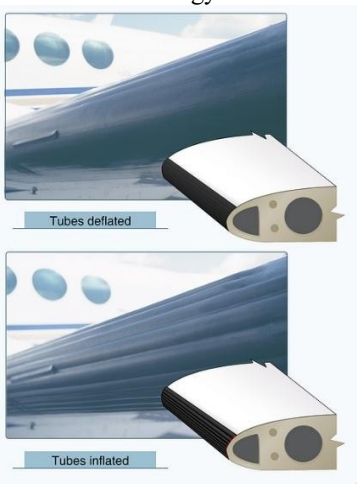



**Figure 2.0-2 Deflated and inflated deicing boots on the LE of the wing** [23]

*Systems for Chemical Ice Protection*

Chemical techniques lower the freezing point and impair ice adhesion by allowing fluids based on glycol to permeate porous surfaces. These systems are better suited for tiny aircraft because they are lightweight but have a limited endurance [13].



**Figure 2.0-4 Type IV fluid applied by operator on the wing of the plane** [24]

Every IPS strategy has compromises. Mechanical solutions lower energy consumption but can be less dependable chemical systems are straightforward but have a time restriction electrothermal systems provide precision but have high electrical demands and bleed -air systems are well-established but energy-intensive. Interestingly, despite its crucial function in stability and control, relatively little research has been done on tailplane protection, despite the fact that IPS for wings, nacelles, and probes has been extensively studied [16].

### 2.3 Engine Exhaust Flow fields as a Heat Source

Turbofan engines' exhaust flow fields are concentrated sources of thermal energy that, in some cases, could help keep ice from accumulating on empennage surfaces. The exhaust gases that depart the core at the nozzle exit usually have high jet velocities of several hundred meters per second and temperatures exceeding 900 degrees Celsius. But as the plume spreads downstream, the jet core cools and becomes diluted due to fast entrainment and mixing with the freestream, which reduces the amount of thermal footprint that actually reaches the tailplane. Engine position, nozzle design, and flying phase all have a significant impact on the amount of heat transmission to the empennage.

From the EASA Type Certificate Data Sheets, representative exhaust characteristics for the A320, G280, and A380 were gathered. Table 1 provides a summary of each engine's critical thrust and exhaust gas temperature parameters. These demonstrate how exhaust energy varies among aircraft classes. The exhaust aligns more closely with the empennage in rear-mounted configurations like the G280, whereas the plume disperses before reaching the tailplane in underwing installations like the A320 and A380. This demonstrates how aircraft design and operational conditions have a significant impact on the viability of employing exhaust heating for tailplane ice protection.

**Table 1 Representative exhaust gas characteristics of selected transport and business jet engines based on EASA Type Certificate Data Sheets** [25], [26], [27]

| Aircraft | Take-off Thrust (kN) | Max Continuous Thrust (kN) | Exhaust Gas Temp. (°C) | Engine Location |
|---|---|---|---|---|
| **Airbus A320** (CFM56-5B) | 98-122 | ~100 | 940-950(TO) | Under-wing |
| **Gulfstream G280** (Honeywell HTF7250G) | 34.5 | 32.6 | >900 | Rear fuselage |
| **Airbus A380** (Rolls-Royce Trent 900) | 340-374 | ~350 | >1000 | Under-wing |

### 2.4 CFD Modelling of Exhaust Flow and Heat Transfer

Investigating exhaust plume tailplane interactions in controlled and repeatable settings is made feasible using computational fluid dynamics, or CFD. In contrast to expensive and challenging experimental investigations in icing settings, CFD enables in-depth examination of temperature, velocity, and turbulence fields in a variety of configurations. The time-averaged distribution of exhaust temperature and momentum can be ascertained in this situation using steady -state simulations, but dynamic events like throttle changes, gust encounters, or plume oscillations are frequently studied using transient simulations.

In order to generate high-quality structured grids for transonic wing analysis, Li Liajin used ANSYS ICEM in recent aerodynamic studies. These meshes showed increased accuracy in capturing the laminar turbulent transition. In exhaust plume investigations, where grid refinement close to shear layers controls the precision of convective heat transfer predictions, such meshing techniques are equally pertinent. Because of its established trustworthiness in aerothermal analysis, ANSYS Fluent is used as the flow solver in this study. Fluent offers strong capability for both steady and transient simulations and integrates sophisticated turbulence models, such as Li's Transition SST model. Prior to interpreting temperature fields, heat flux, or surface heating potential, residuals below $10^{-4}$ are typically considered an acceptable level numerical convergence is still required for trustworthy results.

**Table 2 Roles of ANSYS ICEM and ANSYS Fluent in CFD studies of external aerodynamics and exhaust flow fields**

| Tool | Primary Function | Strengths | Role in Current Research |
|---|---|---|---|
| **ANSYS ICEM** | Mesh generation | Structured/unstructured grids, strong control of refinement, good for boundary layers. | Used by Li Liajin for accurate meshing of wing transition cases. |
| **ANSYS Fluent** | Flow solver | Robust turbulence models, steady/transient capability, reliable aerothermal results. | Used in this study to simulate exhaust plume-tailplane interaction. |

### 2.5 Aircraft Geometry Considerations

Geometric integrity has a significant impact on CFD forecast accuracy. The amount that the exhaust plume hits or avoids the tailplane depends on the engine location, tailplane location, and fuselage interaction. The CFM56-5B engines installed under the wings of the Airbus A320 prevent direct heating by discharging exhaust plumes far below the horizontal tailplane. In contrast, the Gulfstream G280's Honeywell HTF7250G engines, which are placed in the rear fuselage, drive exhaust closer to the tailplane, perhaps increasing thermal exposure. The Rolls-Royce Trent 900 engines that power the Airbus A380 are a wide-body aircraft with substantial fuselage wake interactions and huge underwing engines.

These three aircraft collectively offer representative CFD analysis test cases. The A380 shows the enormous scale of very large transport aircraft, the G280 symbolizes business jets with fuselage-mounted power, and the A320 displays a traditional single-aisle design with underwing engines. Their inclusion makes it possible to systematically evaluate the effects of engine shape and installation on the possibility that exhaust heating will contribute to tailplane ice protection. These models were downloaded from GrabCAD [28], [29], [30].




**Figure 2.05 CAD Models of A320, G280 & A380**

### 2.6 Summary of Research Gap

According to the literature, engine exhaust gases have a considerable amount of thermal energy, but this potential quickly degrades because of ambient mixing and plume expansion. Few studies have examined the relationship between exhaust plumes and empennage surfaces, despite the fact that CFD has been frequently used to simulate hot-air anti-icing of wings and nacelle lips. Furthermore, it is not possible to determine if exhaust heating alone can adequately protect the tailplane by conducting a systematic comparison across various aircraft designs or operating phases. Because of this paucity of data, it is difficult to say if passive exhaust heating is a practical safety precaution or if specialized tailplane ice prevention devices are still necessary to ma intain certification standards.

## 3.0 CFD Pre-Processing and Setup

### 3.1 Introduction to Pre-Processing

The model needs to be well-prepared before any flow simulations are undertaken in order to effectively represent the physical issue while yet being computationally efficient. Any CFD study starts with this preparation, also referred to as pre-processing. Creating a representational geometry, meshing the domain, and implementing appropriate boundary conditions are the three primary tasks involved. The dependability of the ensuing findings is directly impacted by this factor.

For this study, pre-processing was completed for the Airbus A320, Gulfstream G280, and Airbus A380 aircraft. They were chosen because they offer a useful contrast in engine size and layout, which has a direct impact on the way exhaust plumes interact with the tailplane. An excellent example of the typical narrow-body design is the A320's CFM56-5B underwing engines. An example of exhaust jets directed closer to the tailplane may be seen in the Honeywell HTF7250G engines located in the rear fuselage of the G280. The A380, a massive transport plane with Rolls-Royce Trent 900 engines has 4 high-thrust underwing engines. The impact of engine form and placement on the exhaust heating potential of the tailplane have been compared in Table 3. Also the Figure 3.0-1, Figure 3.0-2 & Figure 3.0-3 shows the exhaust plume direction in all the aircrafts.

The following sections explain the steps taken to build the models for these aircraft: geometry definition, mesh generation, and boundary condition setup. These pre-processing tasks ensure that the CFD domains are realistic enough to reflect aircraft behaviour, while also being manageable for stable and accurate solutions in ANSYS Fluent.




**Figure 3.0-1 Airbus A320 with underwing-mounted CFM56-5B engines exhaust plume directed below the tailplane** [31]**.**




**Figure 3.0-2 Gulfstream G280 with rear-fuselage-mounted HTF7250G engines plume aligned with the tailplane** [32]**.**




**Figure 3.0-3 Airbus A380's Rolls-Royce Trent 900 engines plume spread but exhaust remains directed below the tailplane** [33]

**Table 3 Engine models and mounting characteristics of the three aircraft**

| Aircraft | Engine Model | Mounting Location | Tailplane–Engine Relationship |
|---|---|---|---|
| **Airbus A320** | CFM56-5B | Underwing | Plume directed below tailplane (limited interaction) |
| **Gulfstream G280** | Honeywell HTF7250G | Rear fuselage | Plume aligned with tailplane (direct exposure) |
| **Airbus A380** | Rolls-Royce Trent 900 | Large underwing | Plume expands under empennage (reduced direct heating) |

### 3.2 Assumptions

To make the computational setup simpler while maintaining the results' representativeness of exhaust–tailplane interactions, a number of assumptions were included. With the energy equation enabled, air was assumed to be the working fluid and modelled as a compressible ideal gas. The International Standard Atmosphere (ISA) tables at the appropriate flight altitudes were used to determine the temperature, air density, and static pressure for cruising phases. Instead of modelling combustion effects and species composition in the exhaust, the EASA Type Certificate Data Sheets were used to prescribe the nozzle outlet with total velocity and temperature values.

The fuselage and tailplane were among the solid limits that were classified as stationary walls with a no-slip shear condition. In accordance with traditional aircraft design, aluminium was assumed to be the structural material however, this was simply a nominal assumption because conjugate heat transfer (CHT) across the structure was not modelled. Convective heating of external surfaces was thus the exclusive focus of the analysis.

Only the area of the aircraft downstream of the engine nozzle was included in the reduced computational domains. To maintain the proper spatial relationship between the nozzle and the tailplane, just a small portion of the centre fuselage was kept the forward fuselage, wings, and the majority of the centre fuselage were removed. This prevented needless mesh complexity while guaranteeing that computational resources were allocated to the area of interest.

It should be mentioned that while a number of alternative aircraft configurations were initially considered, not all of the CAD models that were accessible from sources like GrabCAD were appropriate for models of the aircraft. They were simplified in Fusion360. Because their models were adequately waterproof and depict three different aircraft types, the Airbus A320, Gulfstream G280, and Airbus A380 were chosen.

Lastly, the study's focus was restricted to determining the temperature and velocity fields and how these affected the tailplane surface. Since the goal was to evaluate the viability of exhaust heating as an additional protective mechanism on cold days, no explicit icing accretion physics were included. Time-averaged distributions were calculated using steady-state simulations, and unstable plume behaviour was specifically examined using transient runs.

### 3.3 Aircraft Geometry and Domain Design

For the purpose of representing three different aircraft types with different engine locations, the computational domains were created for the Airbus A320, Gulfstream G280, and Airbus A380. Using underwing CFM56-5B engines, the A320 is a narrow-body aircraft that exemplifies the traditional single-aisle design. An example of a business jet having exhaust plumes that are more closely aligned with the tailplane is the G280, which has Honeywell HTF7250G engines positioned on the rear fuselage. An example of the scale impacts of high-thrust underwing installations is the A380, a very large transport aircraft with Rolls-Royce Trent 900 engines. In order to evaluate how engine location affects the possibility of exhaust heating reaching the tailplane, these opposing layouts were selected.

Minor geometric characteristics like antennae, flap track fairings, and minute surface details were eliminated to save computing time. Due to their dominance in the exhaust–tailplane interaction, the modelling only kept the fuselage, engines, and tailplane. To reduce the domain size by half without sacrificing physical precision, a symmetry plane was added along the centreline of the fuselage. In order to allow exhaust plume formation and entrainment to organically evolve prior to reaching the outlet plane, the computational domains were sufficiently expanded upstream, downstream, and laterally.

Computing domains created in ANSYS Design Modeler are displayed in the below figures. In the A320 domain Figure 3.0-4, the horizontal tailplane's position in relation to the exhaust plume and the engines situated under the wings are prominent. One layout of special interest for evaluating possible exhaust heating effects is the G280 (Figure 3.0-5), where the rear-fuselage-mounted engines are situated near to the tailplane. In order to save computing expense, the A380 domain (Figure 3.0-6) maintains a symmetry plane along the fuselage while displaying the enlarged enclosure needed to capture the massive exhaust plumes produced by the Trent 900 engines.

Instead of incorporating the complete forward fuselage and wing system, the models were trimmed at the engine nozzle exit to further maximize computational efficiency. Since this study is only concerned with exhaust plume generation and its thermal interaction with the tailplane, adding upstream geometry would significantly raise computing costs without adding any new physical knowledge. Using Boolean feature, the model is subtracted out of the fluid domain this decreases the computational duration. Additionally, by focusing computing resources on the tailplane region which has received relatively little attention in earlier research this method immediately fills the research gap mentioned in 1.3 Research Gaps.

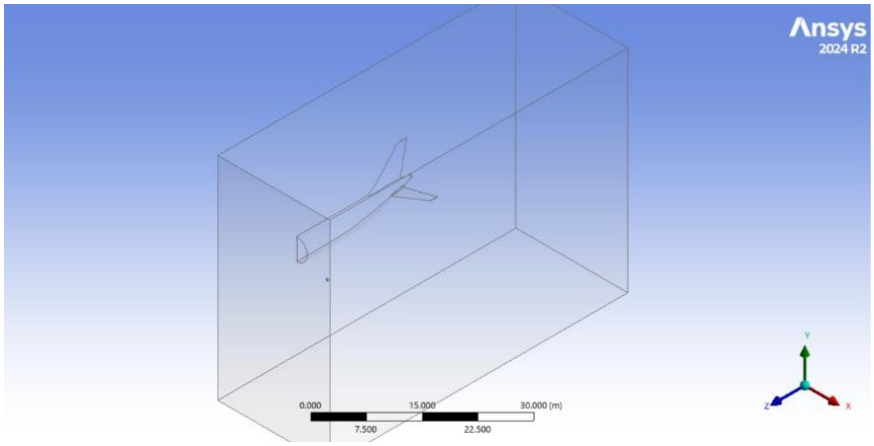



**Figure 3.0-4 Computational domain of the Airbus A320 with underwing engines and symmetry applied.**

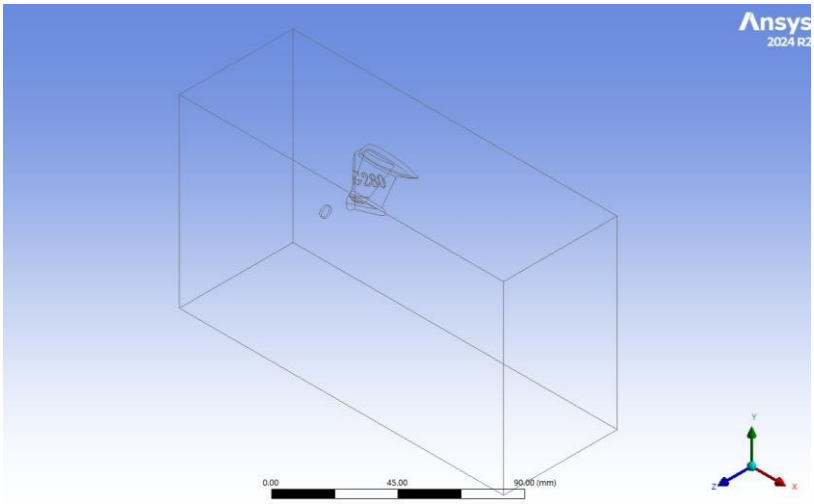



**Figure 3.0-5 Computational domain of the Gulfstream G280 with rear-fuselage engines aligned with the tailplane.**

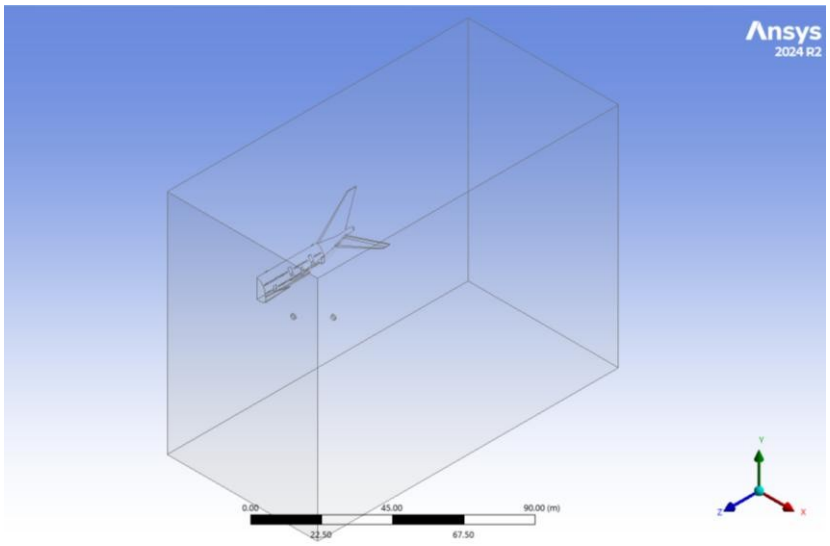



**Figure 3.0-6 Computational domain of the Airbus A380 with large underwing engines and extended enclosure.**

Together with the images, a comparative overview of the computing domains for each aircraft is given in Table 4. It enumerates the symmetry conditions, the simplifications used during geometry preparation, and the approximate domain dimensions. The A320 and A380 needed larger enclosures because of their underwing engine location, whereas the G280 was modelled with a relatively small domain cantered around its rear-mounted engines. This table helps illustrate how domain size was scaled to fit aircraft class and thrust level. In order to ensure that plume formation and tailplane contact could be examined under representative geometric conditions, the figures and table collectively show how each aircraft was prepped for CFD research.

**Table 4 Computational domain dimensions, symmetry, and simplifications for the three aircraft.**

| Aircraft | Engine Model | Domain Size (approx.) |
|---|---|---|
| **Airbus A320** | CFM56-5B | 30 m × 30 m × 35 m |
| **Gulfstream G280** | Honeywell HTF7250G | 130 mm × 60 mm × 60 mm |
| **Airbus A380** | Rolls-Royce Trent 900 | 80 m × 80 m × 90 m |

### 3.4 Meshing Strategy in Fluent

The Airbus A320, Gulfstream G280, and Airbus A380 domains meshes were generated using ANSYS Fluent. Since it offers versatility in discretizing complex geometries like the fuselage, tailplane, and empennage area, an unstructured tetrahedral mesh was used in all situations. In order to keep the mesh size controllable without sacrificing the flow field's physical integrity, a symmetry plane was added along the fuselage centreline to shrink the computational domain.

Refinement was concentrated on the horizontal tailplane faces since they are the primary focus of this study. While the rest of the domain was meshed more coarsely, these surfaces were discretized with smaller element sizes to improve the resolution of nea r-wall flow and surface heat transfer properties. This chosen to increase allowed computer resources to be allocated to the tailplane,

where accurate temperature distribution forecasting is critical for assessing exhaust heating impacts.

Since the goal of the current work is to achieve numerical convergence rather than experimental validation, it should be highlighted that a mesh independence investigation was not conducted. Instead of comparing CFD results with reference data, the goal is to get stable and consistent solutions for plume–tailplane interactions under specified boundary conditions. Therefore, element skewness (maintained below 0.9) and the use of inflation layers to sufficiently resolve near-wall gradients on the tailplane were used to guarantee mesh quality.

The total mesh of each computational domain as seen along the symmetry plane is displayed in the below figures.

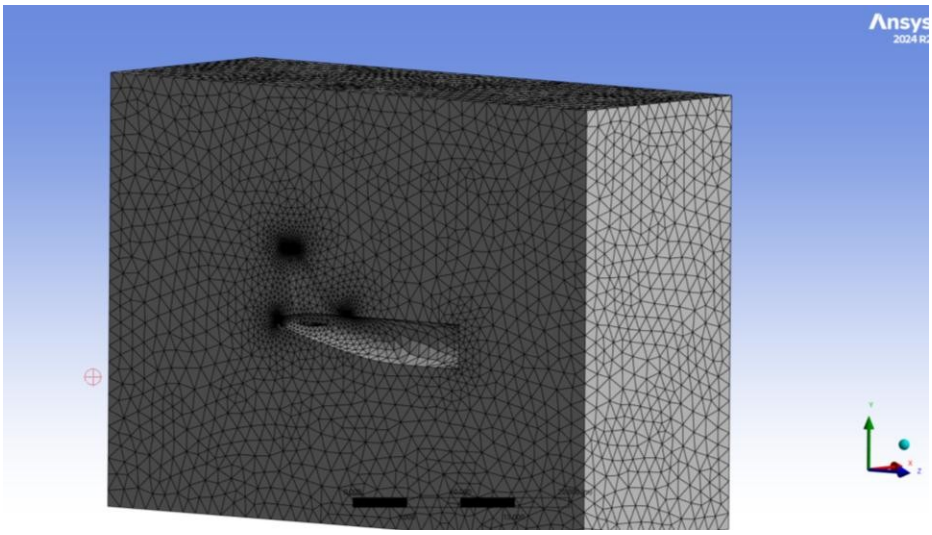


**Figure 3.0-7 Overall mesh of the Airbus A320 computational domain viewed along the symmetry plane.**

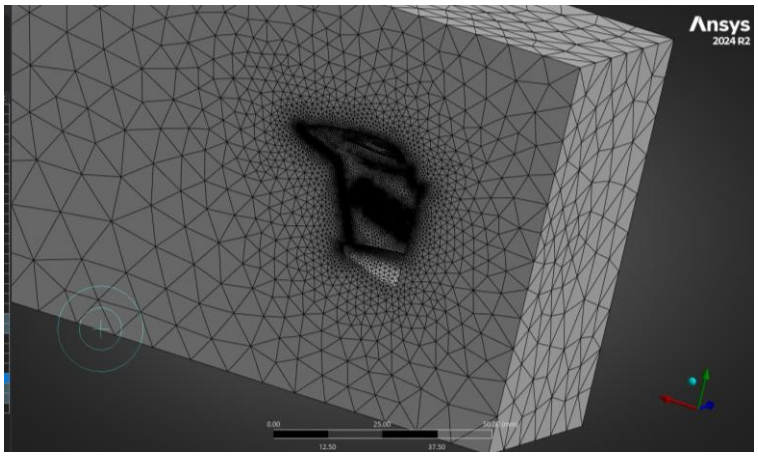



**Figure 3.0-8 Overall mesh of the Gulfstream G280 computational domain viewed along the symmetry plane.**

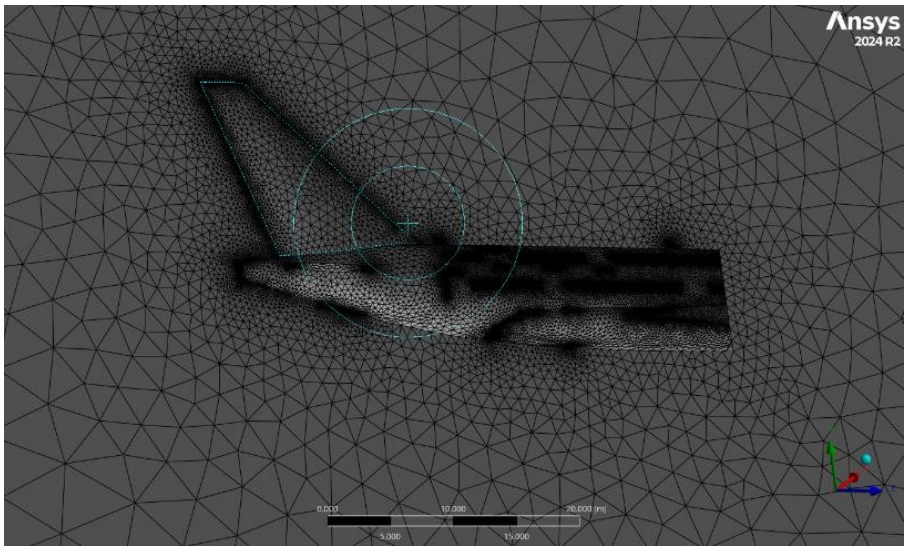



**Figure 3.0-9 Overall mesh of the Airbus A380 computational domain viewed along the symmetry plane.**

Additionally, the chosen aircraft's each tailplane faces were given a finer mesh scaling, it is shown in Figure 3.0-7 - Figure 3.0-9. These show how the meshing technique is the same for all three aircraft configurations.

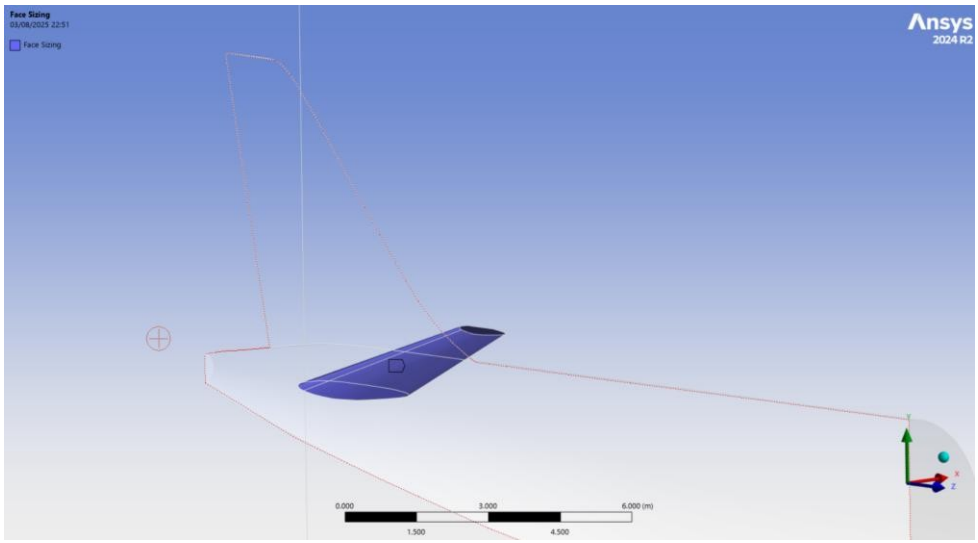



**Figure 3.0-10 Tailplane faces of the Airbus A320 assigned finer mesh sizing for improved local resolution.**

.

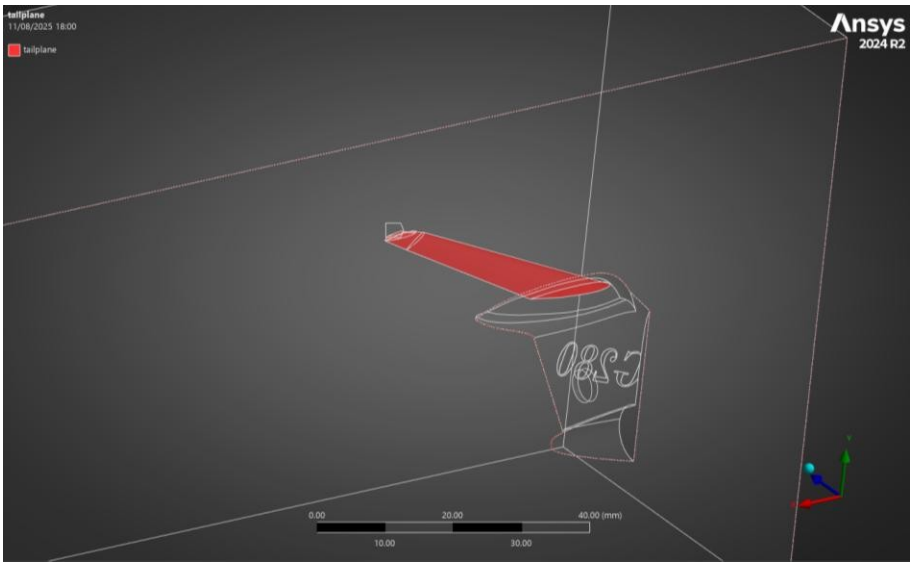



**Figure 3.0-11 Tailplane faces of the Gulfstream G280 discretised with finer surface mesh.**

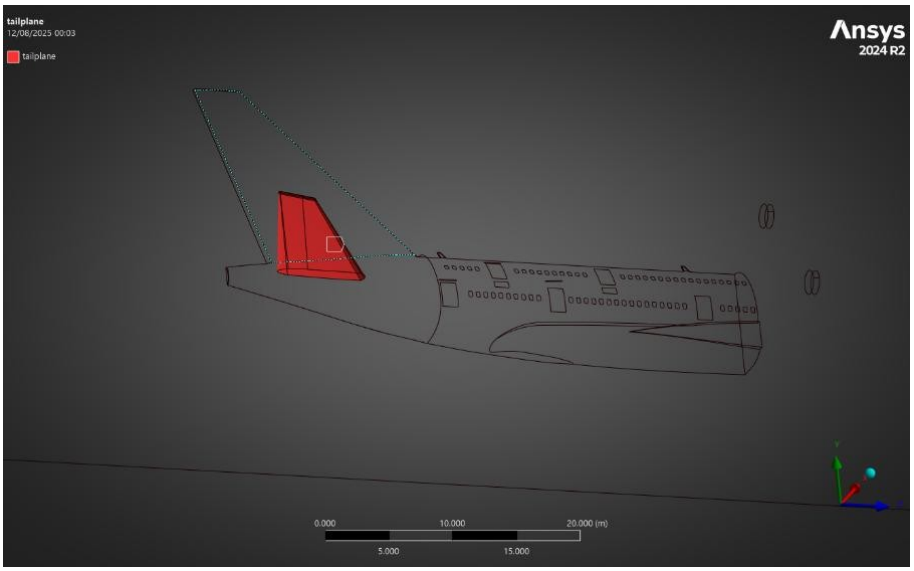



**Figure 3.0-12 Tailplane faces of the Airbus A380 meshed with local refinement to capture heat transfer gradients.**

Furthermore, the mesh statistics for the three computing domains are summarized in Table 5. Along with the maximum skewness and a remark on the tailplane refinement used, it gives an estimate of the number of nodes and elements created. Although the overall mesh densities vary depending on the size of the aircraft, this table shows that all three domains kept quality metrics within reasonable bounds (skewness < 0.9) and that refinement was always focused on the tailplane faces to improve local resolution.

**Table 5 Mesh statistics for A320, G280, and A380 computational domains, showing refinement at the tailplane faces and overall mesh quality.**

| Aircraft | Nodes | Elements | Tailplane Refinement Applied |
|---|---|---|---|
| **Airbus A320** | 122702 | 677078 | Face Sizing element size 0.5m |
| **Gulfstream G280** | 104576 | 566012 | |
| **Airbus A380** | 154178 | 845359 | |

This meshing strategy aligns with the scope of the study, which is to evaluate exhaust heating feasibility at the tailplane. As such, convergence-focused simulations were prioritised over validation, and mesh quality was ensured through targeted refinement and monitoring rather than independence testing.

### 3.5 Boundary Conditions

For the three chosen aircraft, boundary conditions were used to simulate authentic operating settings. The International Standard Atmosphere (ISA) at the appropriate altitude was used to determine the velocity, density, temperature, and static pressure values that were prescribed for the freestream inlet. The design Mach number and the associated local speed of sound were used to determine the freestream velocity for cruise phases. According to the EASA Type Certificate Data Sheets, the engine nozzle inlet was classified as a velocity inlet, and its total temperature and velocity were calculated using the engine exhaust gas temperature (EGT) and nozzle performance data.

The outlet was modelled as a pressure outlet and set to ISA static pressure at the flight altitude. Solid surfaces, such the fuselage and tailplane, were treated as stationary aluminium walls with a no-slip shear condition in compliance with the assumptions in Section 3.2. A symmetry plane was imposed along the fuselage's centreline in order to reduce the computational domain while preserving flow fidelity.

Figure 3.0-13 shows the setting of the computational domain for ANSYS Fluent. The enclosure incorporates the aircraft's geometry, including the nozzle and tailplane. The blue face receives the freestream inlet, while the red face receives the pressure outlet. This demonstrates how each simulation uses a realistic boundary condition configuration; this is similar for all cases.

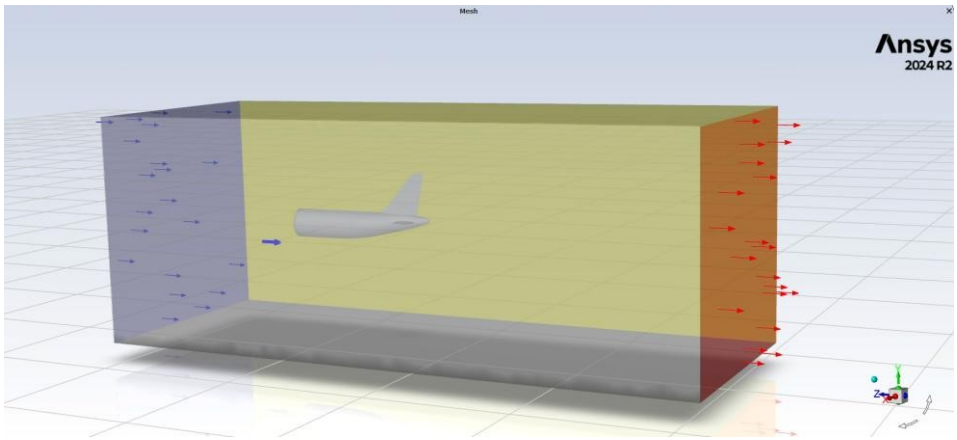



**Figure 3.0-13 Computational domain in ANSYS Fluent showing the freestream inlet (blue), engine exhaust(single blue), pressure outlet (red) and aircraft geometry positioned within the enclosure. A symmetry plane is applied along the fuselage centreline to halve the domain size.**

### 3.5.1 Cruise Condition Cases

All three aircraft were subjected to cruise circumstances in order to compare the exhaust-tailplane interaction. The A320, G280, and A380's freestream and nozzle conditions are listed in Table 6. The freestream values were calculated from the design Mach number and ISA conditions at the respective altitude, while the nozzle inlet parameters were obtained from certified engine data.

These relations were used to calculate the Freestream Velocity and Nozzle Velocity in Table 6 for the A320, G280, and A380 from Mach and temperature:

- Freestream :

$$V_\infty = M \cdot a = M \cdot \sqrt{\gamma R T_\infty} \quad (1)$$

- Nozzle(engine jet) :

$$V_e = M \cdot a = M \cdot \sqrt{\gamma R T_e} \quad (2)$$

where:
$V_\infty$ = Freestream velocity (m/s)
$V_e$ = Nozzle (engine_inlet) velocity (m/s)
$M$ = design cruise Mach number
$a$ = speed of sound at flight altitude
$\gamma$ = ratio of specific heats (1.4 for air)
$R$ = specific gas constant for air (287 J/kg·K)
$T_\infty$ = ambient static temperature from ISA (K).
$T_e$ = engine exhaust temperature from EASA datasheet (K).

**Table 6 Cruise-phase boundary condition values for the A320, G280 and A380**

| Parameter (Cruise) | A320 (CFM56-5B) | G280 (HTF7250G) | A380 (RR Trent 900) |
|---|---|---|---|
| Altitude | FL350 (35,000 ft) | FL450 (45,000 ft) | FL350 (35,000 ft) |
| Design Mach number | 0.78 | 0.85 | 0.85 |
| Nozzle temperature $T_e$ (K) | 1188.15 | 1173.15 | 1123.15 |
| Nozzle velocity $V_e$ (m/s) | 538.933 | 583.58 | 571.008 |
| Freestream temperature T∞ (K) | 218.85 | 216.65 | 218.85 |
| Freestream velocity V∞ (m/s) | 231.298 | 250.835 | 252.056 |
| ISA density ρ∞ (kg·m$^{-3}$) | 0.3796 | 0.2371 | 0.3796 |
| ISA static pressure p∞ (kPa) | 23842 | 14748 | 23842 |

This table illustrates how variations in engine design and altitude can affect both freestream and exhaust jet conditions. The A380 and A320 share a FL350 but have different nozzle velocities because of thrust class, while the G280 runs at a higher altitude (FL450), which results in a lower air density but a higher freestream velocity at Mach 0.85.

### 3.5.2 Multi-Phase Conditions for A320

The A320 was also simulated in four stages: taxi, runway roll, take-off, and cruise in order to assess how sensitive exhaust heating is to operating circumstances. On chilly days, the taxi and runway phases were set at ground level, and take-off denoted maximum thrust operation. Cruise values are in line with the design Mach condition at FL350. Table 7 provides a summary of these boundary conditions.

**Table 7 Multi-phase boundary condition values for the A320.**

| Parameter | Taxi (Idle) | Runway Roll (Breakaway) | Take-off (MTO) | Cruise (FL350) |
|---|---|---|---|---|
| Altitude | SL | SL | SL | FL350 |
| Freestream Temp. (K, ISA) | 278.0 | 278.0 | 278.0 | 218.85 |
| Freestream Velocity (m/s) | 10.3 | 0 | 80.0 | 231.298 |
| Density (kg/m³, ISA) | 1.225 | 1.225 | 1.225 | 0.3796 |
| Pressure (kPa, ISA) | 101325 | 101325 | 101325 | 23842 |
| Nozzle Temp. (K, EGT) | 333.0 | 333.0 | 400.0 | 1188.15 |
| Nozzle Velocity (m/s) | 30.0 | 30.0 | 107 | 538.933 |

When combined, Table 6 and Table 7 define the boundary conditions used in this study. While the G280 and A380 were only evaluated while cruising, the A320 was evaluated in multiple stages to capture the effect of forward velocity and thrust setting on exhaust–tailplane interaction. This organized approach ensures aircraft comparability while also providing deeper insights into operational variability for the A320.

# 4.0 CFD Solution Strategy and Post-Processing

## 4.1 Solver Setup in ANSYS Fluent

A pressure-based, steady RANS formulation with absolute velocity and (where indicated) gravity enabled to reflect ground-phase buoyancy was used to solve all instances in ANSYS Fluent (2024 R2). The Transition SST (k–ω) model, which has been demonstrated to successfully capture near-wall behaviour and shear-layer mixing in aerodynamic flows including transition, was used to represent turbulence after the energy equation was triggered.[34]. Air was designated as the working fluid, and ISA conditions at the operating altitude were used to specify the density, pressure, and temperature for each case. In accordance with earlier ice protection CFD studies, solid boundaries (fuselage and tailplane) were given aluminium characteristics for consistency with typical aircraft constructions, even though conjugate heat transport was not resolved [21]. Refer Figure 4.0-1.

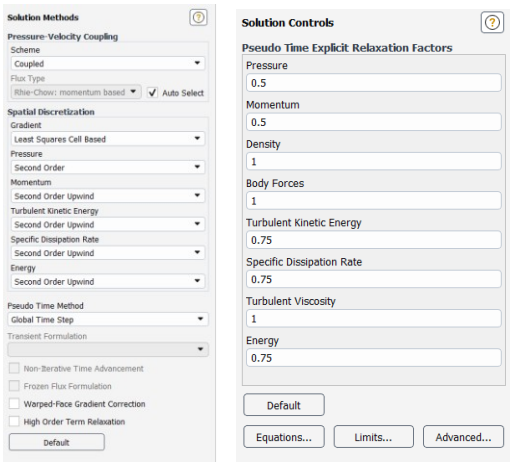



**Figure 4.0-1 Solution Method(left) and Solution Controls(right) for all solved variables**

Definitions of inlets, outlets, and walls were in accordance with 3.5 Boundary Conditions. The computational domain used symmetry to cut costs, and the tailplane and fuselage walls were specified as stationary, non-slip aluminium surfaces.

Run after initialization. Fluent's Standard Initialization was used to initialize the simulations from the freestream intake. The convergence conditions covered in 4.2 Convergence and Stability Criteria were met by advancing each case for 400 stable iterations.

**Table 8 Summary of Setup Settings**

| Item | Setting |
|---|---|
| **Solver** | Pressure-based, Steady, Absolute velocity |
| **Gravity** | Enabled for ground phases off for cruise unless stated |
| **Models** | Energy = ON Transition SST (k–ω) |
| **Materials** | Air (per case ISA ρ, p, T) Aluminium walls |
| **Coupling** | Coupled (Rhie–Chow momentum-based) |
| **Gradients** | Least-Squares Cell-Based |
| **Discretisation** | Second-Order Upwind (p, U, k, ω, Energy) |
| **Initialization** | Standard, Compute from inlet |
| **Iterations** | 400 for cruise conditions & 200 for multi-phase conditions |

### 4.2 Convergence and Stability Criteria

In every instance, convergence was assessed using both physical monitors and numerical residuals. In accordance with standard procedure in aerothermal CFD investigations, the scaled residuals for continuity, momentum, turbulence, and energy equations had to be less than $10^{-4}$ [1], [2]. After about 400 iterations for cruise condition cases and 200 iterations for multiphase A320 cases, the energy residual stabilized close to the $10^{-4}$ threshold, while the momentum and turbulence residuals usually decreased to the $10^{-5}$-$10^{-6}$ range.

The area-weighted average temperature over the horizontal tailplane was used as a physical monitor to augment the residuals. This confirmed that the thermal interaction between the plume and the tailplane had stabilized. Only after the monitor's oscillations were contained to less than 0.1 K and it reached a steady asymptote was convergence allowed.

It took an average of 400 iterations to achieve convergence across all aircraft and phases. For transparency, complete residual histories and monitor plots are provided in the Results chapter.

**Table 9 Convergence and stability criteria aligned with numerical results.**

| Criterion | Target / Observed Result |
|---|---|
| Continuity residual | $\leq 1.0 \times 10^{-4}$ (stabilised ~$10^{-5}$) |
| Momentum residuals (x,y,z) | $\leq 1.0 \times 10^{-4}$ (typically ~$10^{-5}$–$10^{-6}$) |
| Turbulence residuals (k, ω) | $\leq 1.0 \times 10^{-4}$ (converged to $10^{-5}$ range) |
| Energy residual | $\leq 1.0 \times 10^{-4}$ (stabilised near threshold by 350–400 iterations) |
| Monitor (thermal) | Area-weighted tailplane temperature, steady within ±0.1 K |

### 4.3 Post-Processing Approach

Post-processing was performed in ANSYS CFD-Post to extract both qualitative and quantitative insights from the converged flow fields. A combination of surface, plane, and volumetric analyses was used to evaluate the behaviour of the exhaust plume and its interaction with the tailplane.

Surface contours of static temperature were generated on the tailplane to assess the extent of thermal exposure. These enabled a direct evaluation of whether the exhaust plume could deliver sufficient heating to prevent ice accretion under cold-day conditions. Streamlines were seeded from the nozzle exit and coloured by velocity magnitude to visualise plume trajectory, entrainment, and mixing with the freestream. This provided insight into whether the exhaust reached the empennage under different aircraft configurations and flight phases. Static temperature contours were assessed on planar slices that were placed along the exhaust axis and downstream areas. In order to ascertain whether high temperatures continued up to the tailplane, these aircraft were utilized to monitor plume thermal decay.

Furthermore, the overall extent and mixing behaviour of the exhaust plume inside the computational area were captured by using volumetric visualization of the flow field. This method offered a worldwide perspective of the plume's thermal footprint, which enhanced the localized investigation on surfaces and planes. The Results chapter provides a detailed presentation and discussion of these indicators.

# 5.0 Result & Discussion

## 5.1 Convergence and Stability Results

### 5.1.1 Cruise Condition Cases

Figure 5-1 displays a representative residual history for the A320 cruise state. Out of all the airplanes and phases, this case was chosen because it had the most distinct residual degradation pattern. The energy residual stabilized around $10^{-4}$ after around 400 iterations, but the continuity, momentum, and turbulence residuals declined progressively to the order of $10^{-5}$ & $10^{-6}$. Although the taxi and runway roll conditions converged more slowly because of the reduced exhaust momentum, similar behaviour was seen in the G280 and A380 cruise cases as well as the A320 multi-phase situations.

The G280 cruise case's area-weighted average tailplane temperature monitor, which was selected as the most representative thermal monitor of all the cases, is shown in Figure 5-2. After about 50 iterations, this plot settled nicely to a steady asymptote within ±0.05 K, with little volatility for the rest of the experiment. With just slight variations in the amplitude of the initial transient, equivalent monitors for the A320 and A380 showed the same general pattern.

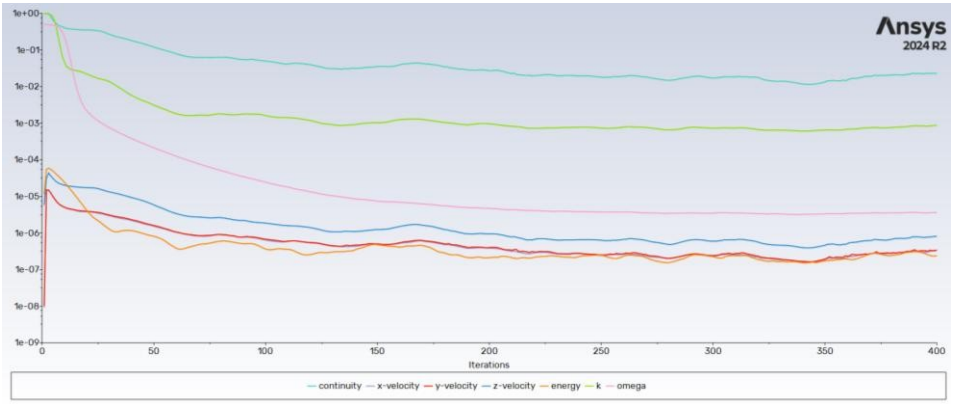



**Figure 5-1 Residual history for the A320 cruise case, representative of the best residual convergence among all simulations**

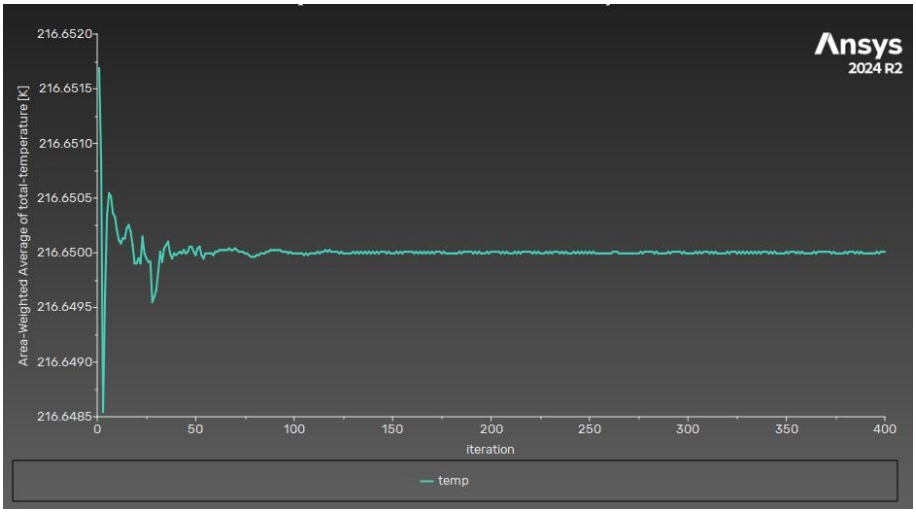



**Figure 5-2 Area-weighted average tailplane temperature for the G280 cruise case, representative of the best thermal monitor across all cases**

While the full set of residuals and monitor charts for every scenario is included in the Compliance of all Residual and Temperature for completeness, these two examples are shown here as the best convergence graphs across all aircraft and phases.

### 5.1.2 Multi-phase Conditions for A320

Four different stages were used to evaluate the convergence behaviour of the A320: take-off, cruising, runway roll, and taxiing. The take-off case, shown in Figure 5-3, was chosen as the best example since it featured the most consistent and identifiable convergence profile out of the four. After about 300 iterations, the energy residual stabilized at $10^{-5}$, but the continuity, momentum, and turbulence variables decreased to the order of $10^{-5}$ & $10^{-6}$. Throughout the first 50 iterations, the residuals rapidly decreased. Following the initial transient, the associated tailplane temperature monitor (Figure 5-4) displayed a smooth asymptotic approach to steady state, with fluctuations remaining within ±0.2 K of the mean.

Although there were noticeable variations in the rate of convergence, the other phases showed comparable behaviour. Because of the low jet momentum and less plume–tailplane interaction during the taxiing phase, convergence occurred slower, and energy residuals flattened earlier but at a greater order of magnitude. Similar behaviour was seen in the runway roll phase, albeit a little quicker convergence was attained as the freestream velocity rose. Overall, the cruising phase scenario exhibited steady behaviour, but it took more iterations (around 400) to get residual levels that were on par with take-off. As a result of reduced exhaust heating at altitude, its temperature monitors stabilized cleanly although at a lower absolute value.

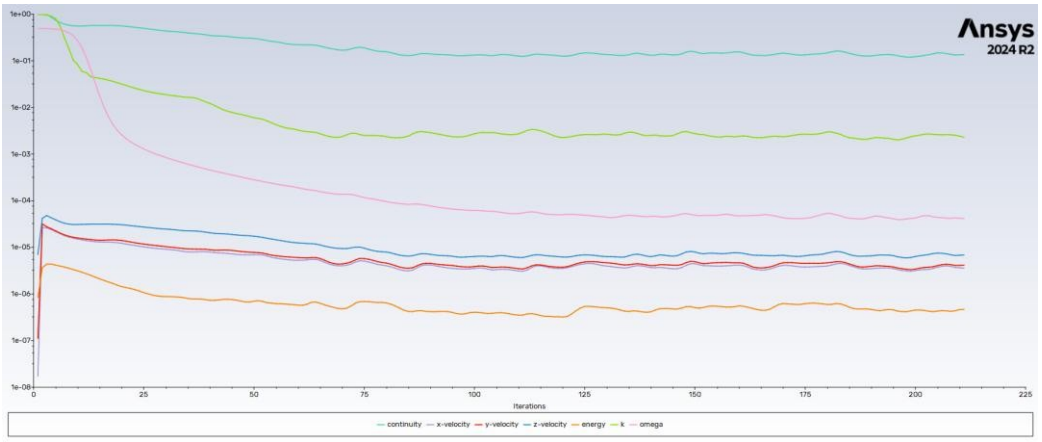



**Figure 5-3 Residual history for A320 take-off case**

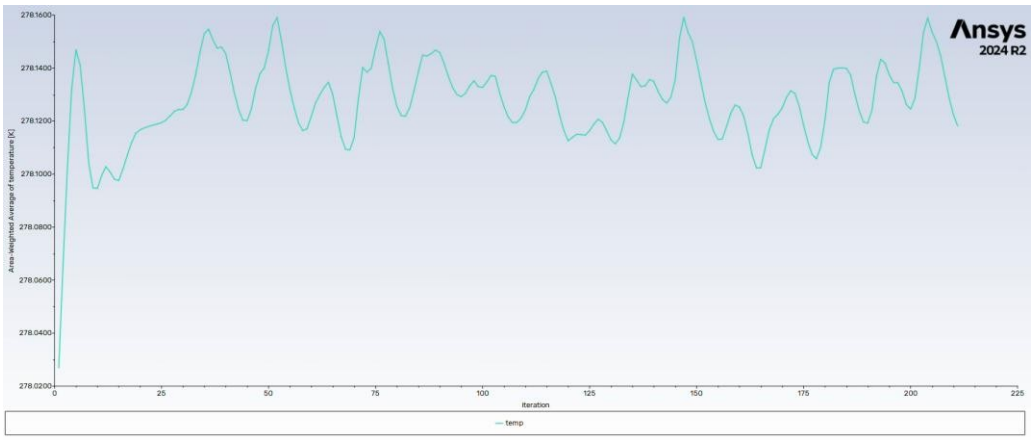



**Figure 5-4 Tailplane temperature monitor for A320 take-off case**

Overall, the trend across all phases showed that higher thrust conditions (cruise, take-off) led to cleaner and faster convergence than low thrust situations (runway roll, taxi). This was consistent with temperature sensors and residual histories, showing that numerical stability is enhanced by increasing jet velocity and plume strength.

## 5.2 Flow Simulation of Exhaust Plume Interaction with Tailplane

### 5.2.1 Cruise Condition Cases

The Gulfstream G280 is the most different of the three aircraft in terms of flow behaviour under cruising conditions, as seen in Figure 5-5. The exhaust plume was directed near the tailplane by the rear-mounted engine design, and the stabiliser was partially impinged upon by the temperature contours and velocity streamlines. As a result, the tailplane surface experienced a discernible, albeit weak, thermal effect.

The Airbus A320 and A380, which both had engines located under their wings, behaved very differently in contrast. In these instances, the exhaust plumes dispersed by quickly mingling with the freestream after passing beneath the tailplane. Despite having a higher thrust, the A380 plume showed more spread, but neither underwing-mounted arrangement resulted in a considerable amount of direct thermal interaction with the tailplane as shown in Figure 5-6

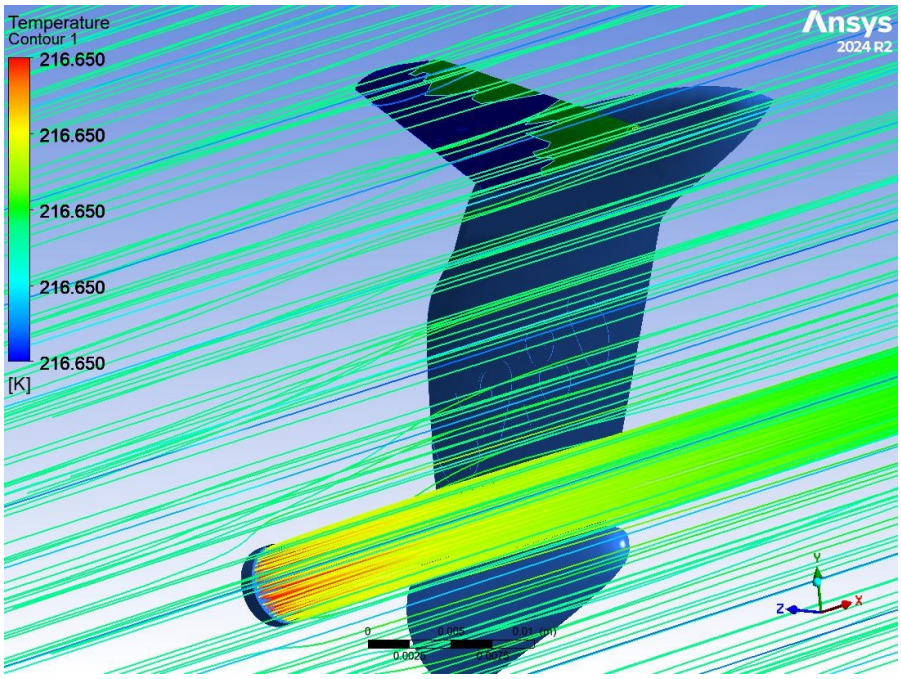



**Figure 5-5 G280 cruise case: rear-mounted exhaust plume impinging on tailplane.**

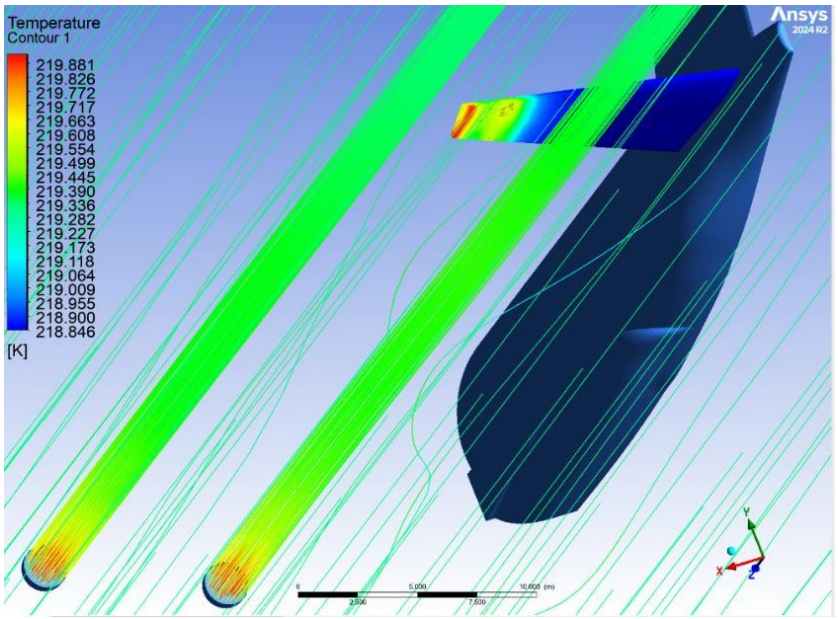



**Figure 5-6 A380 cruise case: exhaust plume impinging on bottom surface of tailplane.**

Thus, the G280 demonstrated the strongest potential for exhaust-induced tailplane heating, while the A320 and A380 showed only indirect effects through entrained flow.

### 5.2.2 Multi-phase Conditions for A320

Among the four multiphase cases, take-off provides the clearest illustration of plume–tailplane interaction. At this phase, the exhaust jet reaches maximum velocity and temperature, allowing the plume to impinge directly on the horizontal tailplane. The temperature distribution shows distinct

heating gradients with localized warming at the trailing edge (Figure 5-7), while the streamline plots demonstrate how exhaust momentum and thermal content combine to alter the surrounding flow field (Figure 5-8).

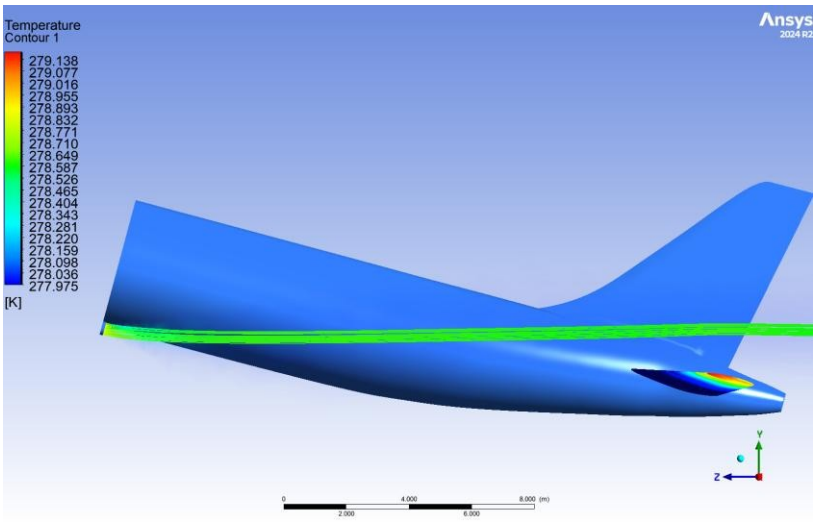



**Figure 5-7 Temperature contour on the A320 tailplane during take-off, showing localized heating at the trailing edge**

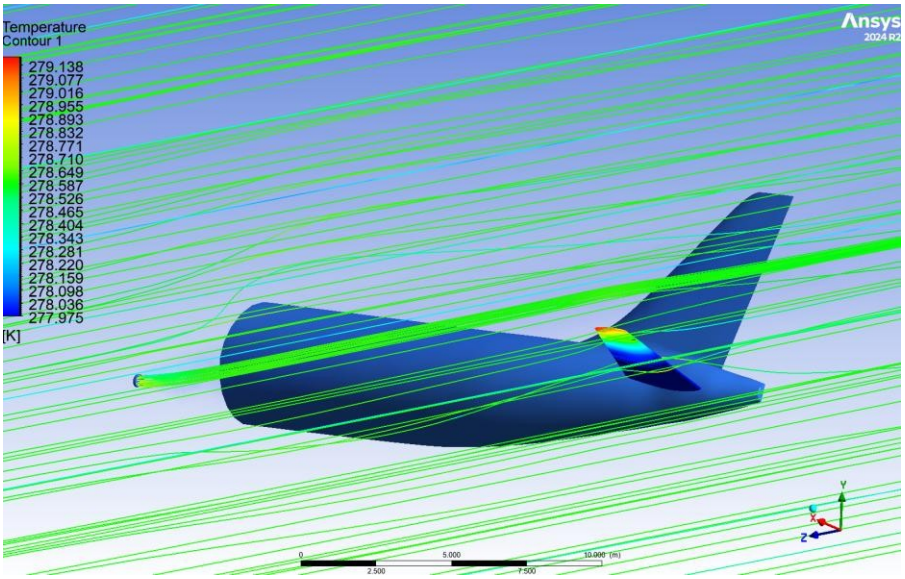



**Figure 5-8 Inlet streamlines superimposed with temperature contours during take-off, illustrating the interaction between the exhaust plume and the tailplane surface.**

By contrast, taxiing and runway roll produce minimal influence, as the weak jet dissipates rapidly into ambient air, leaving the tailplane close to ambient temperature. During cruise, despite the high jet velocity, the dominant freestream carries the plume below the empennage, preventing significant heat transfer. Overall, these results confirm that take-off is the only phase where plume-induced heating is appreciable, underlining its relevance when evaluating exhaust flow as a supplementary ice protection mechanism.

### 5.3 Thermal Influence on the Tailplane Surface

Localized heating occurs on the surface of the A320 during take-off because the engine exhaust plume has enough speed and temperature to reach and interact with the tailplane. The only flight state in which there is direct plume–tailplane interaction is this one. In contrast, there is no discernible impact during the taxiing, runway roll, or cruising phases because the exhaust either dissipates quickly or is convected beneath the empennage by the stronger freestream flow.

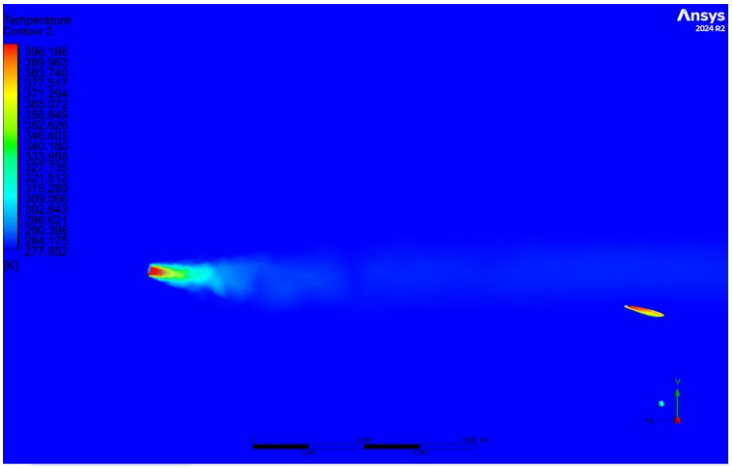



**Figure 5-9 Temperature contour of exhaust gases during A320 take-off phase.**

### 5.4 Comparative Analysis Across Aircraft Configurations

The results of the cruise-condition simulations showed that operating altitude and engine installation geometry have a significant impact on the degree of plume–tailplane contact. There was little direct exhaust influence on the tailplane for the Airbus A320 and A380, both of which had engines located under the wings. Under these arrangements, the plume is vertically displaced beneath the stabiliser and undergoes significant entrainment-induced degradation prior to reaching the empennage.

The Gulfstream G280, on the other hand, which had engines situated on the rear fuselage, behaved very differently. The exhaust plume tightly aligned with the stabiliser due to the low horizontal distance and little vertical offset between the tailplane pla ne and the nozzle output. There was evidence of partial plume impingement on the tailplane, which increased the possibility of thermal influence in comparison to the A320 and A380.

When operational altitude is considered, the A320 and A380 usually cruise at FL350, where there is less chance of prolonged tailplane icing and low ambient temperatures. Consequently, no specific tailplane ice protection system (IPS) is installed on any type. However, the G280 runs at FL450, where plume cooling occurs more quickly and ISA conditions are colder. The G280 has a tailplane IPS in operation since natural exhaust heating is not enough to stop ice buildup in this environment.

**Table 10 Comparative Analysis Summary**

| Aircraft | Engine Location & Geometry | Cruise Condition (Altitude / Mach) | Plume–Tailplane Interaction | IPS Requirement (Service Aircraft) |
|---|---|---|---|---|
| **A320** | Underwing-mounted large horizontal & vertical separation from tailplane | FL350 / M0.78 | Plume dissipates below tailplane negligible heating at stabiliser | No dedicated tailplane IPS |
| **A380** | Underwing-mounted engines positioned slightly aft, but plume remains well below tailplane | FL350 / M0.85 | High-thrust plume spreads widely but does not impinge on tailplane | No dedicated tailplane IPS |
| **G280** | Rear-fuselage-mounted short nozzle–tailplane distance with small vertical offset | FL450 / M0.85 | Plume partially impinges on tailplane strongest thermal influence but plume cools rapidly | Tailplane IPS fitted in service |

### 5.5 Effect of Flight Phase on Exhaust Heating

The flying phase and environmental factors affect exhaust heating efficiency. Due to the jet's high temperature and momentum, the plume may have an impact on the tailplane during take-off; however, during taxiing, runway roll, and cruising, this effect is reduced by freestream convection or fast expulsion. This impact depends on the temperature of the atmosphere; on hot days, convective warming is encouraged by a bigger gradient between the plume and surrounding air, but on cold days, heat transfer is inhibited by a smaller gradient. High moisture content raises the possibility of ice accretion if heating is insufficient, therefore humidity is just as significant as dry air, which speeds up plume mixing. It's necessary to examine these interactions in connection to the CS-25 Appendix C and O icing envelopes to make that exhaust-assisted heating is only considered in authorized atmospheric circumstances.

### 5.6 Discussion of Findings

Exhaust–tailplane interaction is mostly influenced by engine installation and altitude, according to the cruise-condition results. The plumes swiftly dispersed after passing beneath the tailplane of the A320 and A380, which both had underwing engines, leaving little heating behind. Since neither type has a specialized tailplane IPS, this is consistent with operational practice. At normal cruise altitudes (FL350), ice accumulation is already limited by aerodynamic heating and low liquid water content.

With its rear-mounted engines, the G280 acted differently: the plume partially hit the stabilizer and produced a notable heating effect, which quickly subsided at FL450. In accordance with certification requirements for high-altitude business airplanes, an active tailplane IPS is also necessary. All things considered, the study demonstrates that exhaust heating is insufficient to offer trustworthy ice protection. Only during take-off, when exhaust temperature and velocity were at their peak, did heating become a significant factor for the A320. During taxi, roll, and cruise, the plume spread out too rapidly to be of much value. These findings demonstrate the limitations of exhaust heating as a stand-alone technique as well as its potential to support IPS in high-power, low-altitude periods.

## 6.0 Conclusion and Future Work

This study has demonstrated how aircraft configuration and operating philosophy have a significant impact on exhaust–tailplane interactions. The Airbus A320 and A380 cruise-condition simulations showed that engines installed on the underwing produce exhaust plumes that travel beneath the tailplane and quickly disperse with little temperature impact. Therefore, a specific tailplane Ice Protection System (IPS) is not necessary for any type. Their function as high -volume airline aircraft, where reducing structural weight and fuel penalties is critical to economic sustainability, is reflected in this design decision. Because aerodynamic heating and operating altitudes further decrease the risk of ice, avoiding additional IPS hardware lowers operating expenses without sacrificing safety.

In contrast, there was partial plume impingement on the tailplane of the Gulfstream G280, a business jet with engines positioned on the rear fuselage. Despite exhaust heating's inability to ensure natural anti-icing at higher elevations, its design necessitates IPS installation. Private and corporate jets prioritize operational flexibility, safety margins, and passenger assurance over stringent fuel efficiency trade-offs, in contrast to big transport-category aircraft. Thus, the addition of tailplane IPS to such aircraft reflects both consumer expectations and certification compliance.

The comparison also brings an interesting contrast with the Boeing 737, which does use a tailplane IPS despite being the A320's closest rival. This highlightshow two leading manufacturers can follow very different philosophies: Airbus focuses on efficiency and simplicity, while Boeing builds in more redundancy. Both approaches are valid, and the success of both aircraft families shows there is no single answer.

Opportunities to advance this work are evident. Using the same modelling methodology, future research could assess the actual differences in thermal margins between the A320 and B737. Extending the approach to new engine and propulsion systems, like geared turbofans, hybrid - electric concepts, or hydrogen power, where exhaust flows will seem drastically different, would also be beneficial. In order to save energy, hybrid techniques that combine lightweight electrothermal technologies with limited plume heating should also be investigated. Finally, experimental validation using flight data or in an ice tunnel would confirm the results and guarantee certification.

In conclusion, this study demonstrates that underwing-engine aircraft's tailplane cannot be protected by natural exhaust heating alone. It is safe and cost-effective for big airline aircraft, such as the A320 and A380, to not have an IPS. A specific system is required for business jets with rear engines, such as the G280. Instead of using a one-size-fits-all approach, the choice ultimately boils down to aircraft type, mission profile, and design philosophy.

## III.ACKNOWLEDGEMENTS

I would like to sincerely thank Dr. Amir Zare Shahneh for his guidance, patience, and constant encouragement throughout this project. His deep knowledge and clear advice helped me navigate challenges with confidence, while his support and motivation kept m e moving forward. I am truly grateful for the time and effort he dedicated to my work, which played a major role in bringing this project to completion.

## IV.REFERENCES


[1] Don Van Dyke, "POSITION & HOLD an editorial opinion," Aug. 2009.

[2] European Union Aviation Safety Agency (EASA)., "European Union Aviation Safety Agency (EASA). ," 2023.

[3] J. F. Kettle and P. J. Childers, " Tailplane Stall and Icing Effects ," *Springer*, vol. 2nd ed, 2016.

[4] "'Ice Protection System - an overview | ScienceDirect Topics.' https:0//www.sciencedirect.com/topics/engineering/ice-protection-system (accessed Aug. 21, 2025).," ScienceDirect Topics https://www.sciencedirect.com/topics/engineering/ice-protection-system.

[5] P. Fernández-Yáñez, O. Armas, A. Gómez, and A. Gil, "Developing Computational Fluid Dynamics (CFD) Models to Evaluate Available Energy in Exhaust Systems of Diesel Light-Duty Vehicles," *Applied Sciences*, vol. 7, no. 6, p. 590, Jun. 2017, doi: 10.3390/app7060590.

[6] J. P. Clarke and R. B. Jones, "Hybrid Ice Protection Systems for Commercial Aircraft: A Review," *Prog. Aerosp. Sci*, vol. 112, 2020.

[7] M. B. Bragg *et al.*, "Smart Icing Systems for Aircraft Icing Safety," 2002.

[8] German Aerospace Center (DLR) Linder Höhe, "Detecting supercooled water droplets in flight."

[9] A. W. Ross Detwiler, "How to Recover from Tailplane Icing," EnviroTREC .

[10] A. H. Lefebvre and D. R. Ballal, *Gas Turbine Combustion*, 3rd ed. CRC Press, 2010.

[11] Peter Struk, "A Pilot's Guide to Inflight Icing," *NASA Officia*, Oct. 2016.

[12] C. P. Lawson, *Aircraft Icing and Ice Protection Systems*. Cranfield University, 2023.

[13] L. Bennani, P. Trontin, and E. Radenac, "Numerical Simulation of an Electrothermal Ice Protection System in Anti-Icing and Deicing Mode," *Aerospace*, vol. 10, no. 1, Jan. 2023, doi: 10.3390/aerospace10010075.

[14] F. Javed, "Ice Protection and Thermal Management System," Cranfield University, School of Aerospace, Transport and Manufacturing, 2019.

[15] "A330 ICE & RAIN PROTECTION SYSTEM," Aeropeep .

[16] Y. Niu, Z. Wang, J. Su, J. Yao, and H. Wang, "Prediction of Airfoil Icing and Evaluation of Hot Air Anti-Icing System Effectiveness Using Computational Fluid Dynamics Simulations," *Aerospace*, vol. 12, no. 6, p. 492, May 2025, doi: 10.3390/aerospace12060492.

[17] N. Guan, Q. Zhu, W. Chen, and F. Chen, "Numerical Simulation and Optimization of Coupled Hot-Air Anti-Icing Characteristics for a Nacelle Lip," *Aerospace*, vol. 12, no. 7, p. 582, Jun. 2025, doi: 10.3390/aerospace12070582.

[18] D. C. Washington, "NATIONAL TRANSPORTATION SAFETY BOARD AIRCRAFT ACCIDENT REPORT IN-FLIGHT ICING ENCOUNTER AND LOSS OF CONTROL SIMMONS AIRLINES, d."

[19] Admiral Cloudberg, "Into the Valley of Death: The crash of American Eagle flight 4184 and the ATR icing story," Medium.

[20] M. K. Politovich, "Aircraft Icing: A Review of the Issues," 2003.

[21] F. Javed, "Ice Protection and Thermal Management System," Cranfield University, School of Aerospace, Transport and Manufacturing, 2019.

[22] I. Chakraborty, D. N. Mavris, M. Emeneth, and A. Schneegans, "An integrated approach to vehicle and subsystem sizing and analysis for novel subsystem architectures," *Proc Inst Mech Eng G J Aerosp Eng*, vol. 230, no. 3, pp. 496–514, Mar. 2016, doi: 10.1177/0954410015594399.

[23] U.S. Department of Transportation, "Deicing boots on the leading edge of the wing," PICRYL.

[24] Orchidpoet, "De-icing Airplane - stock photo," Getty Images .

[25] T. Certificate Holder, "TYPE-CERTIFICATE DATA SHEET for RB211 Trent 900 series engines," 2022.

[26] No E, "CFM56-5B and CFM56-5C series engines Issue TYPE-CERTIFICATE DATA SHEET for CFM56-5B and CFM56-5C series engines."

[27] Gulfstream Aerospace LP, "TCDS_EASA_IM.A.348_G280_Issue_6," *EASA*, no. 06, pp. 1–15, May 2025.
[28] Jet Trude Mendoza, "Fusion 360 Airbus A380," GrabCAD.
[29] leo zeng, " Gulfstream G280," Grab\cad.
[30] Group 2 CADD 221L - 1-G1, "Airbus A320neo," GrabCAD.
[31] aribus, "A320neo," noticias . Accessed: Aug. 25, 2025. [Online]. Available: https://www.noticia sla ta msa les.com/aircra ft-families/pa ssengers-a ircra ft/a320-family/a320neo/
[32] Dr Dan Saranga, "Gulfstream G280," Blueprnts. Accessed: Aug. 25, 2025. [Online]. Available: https://www.the-blueprints.com/blueprints/modernpla nes/modern - g/73685/view/gulfstream_g280/
[33] NA, "Of white and blue Airbus A380 plane, Airbus A380 Flying, transport, planes png," pngegg. Accessed: Aug. 25, 2025. [Online]. Available: https://www.pngegg.com/en/png-wgdfb
[34] J. Li, "CFD Simulation for a Laminar Flow Wing at M<0.6," Cranfield University, 2018.

# V. Appendices

## A. Ethical Approval Letter

7 March 2025

Dear Mr Chakraborty ,

Reference: CURES/24500/2025
Project ID: 27579
Title: CFD Investigation on Tailplane Ice Protection System

Thank you for your application to the Cranfield University Research Ethics System (CURES).

**We are pleased to inform you your CURES application, reference** CURES/24500/2025 **has been reviewed. You may now proceed with the research activities you have sought approval for.**

If you have any queries, please contact CURES Support.

We wish you every success with your project.

Regards,

CURES Team

## B. Calculations of Boundary Conditions

*Cruise Conditions Cases:*

- *A320(CFM56-5B)*

Freestream :

$$V_\infty = 0.78 \cdot \sqrt{1.4 * 287 * 218.85} = 231.298\, m/s$$

Nozzle(engine jet) :

$$V_e = 0.78 \cdot \sqrt{1.4 * 287 * 1188.15} = 538.933\, m/s$$

- *G280(HTF7250G)*

Freestream :

$$V_\infty = 0.85 \cdot \sqrt{1.4 * 287 * 216.65} = 250.835\, m/s$$

Nozzle(engine jet) :

$$V_e = 0.85 \cdot \sqrt{1.4 * 287 * 1173.15} = 583.58 \text{ m/s}$$

- *A380(RR Trent 900)*

Freestream :

$$V_\infty = 0.85 \cdot \sqrt{1.4 * 287 * 216.65} = 252.056\, m/s$$

Nozzle(engine jet) :

$$V_e = 0.85 \cdot \sqrt{1.4 * 287 * 1123.15} = 571.008 m/s$$

## C. Compliance of all Residual and Temperature Plots

*Cruise Conditions Cases:*

- *A320(CFM56-5B)*

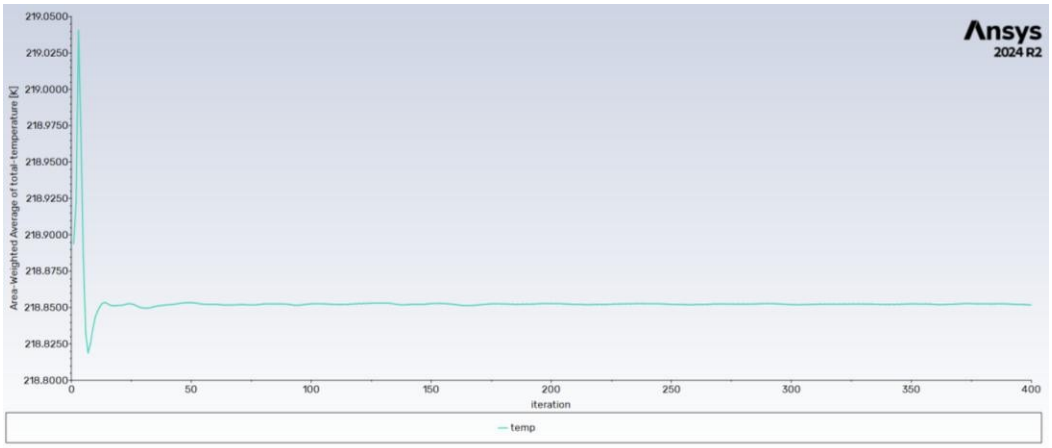



**Figure C-1 Area-weighted average tailplane temperature for the A320 cruise case**

- *G280(HTF7250G)*

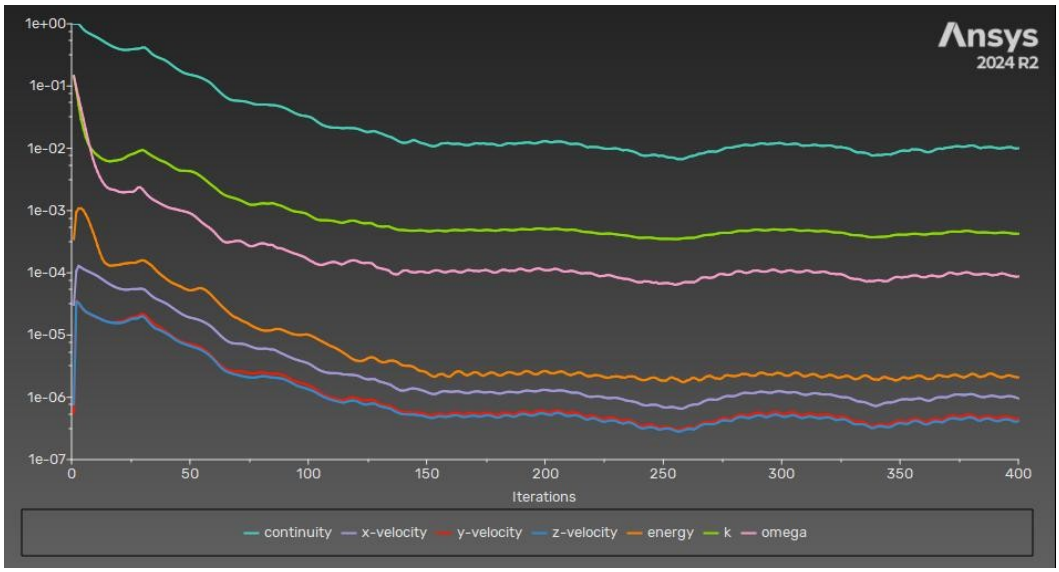



**Figure C-2 Residual history for the G280 cruise case**

• *A380(RR Trent 900)*

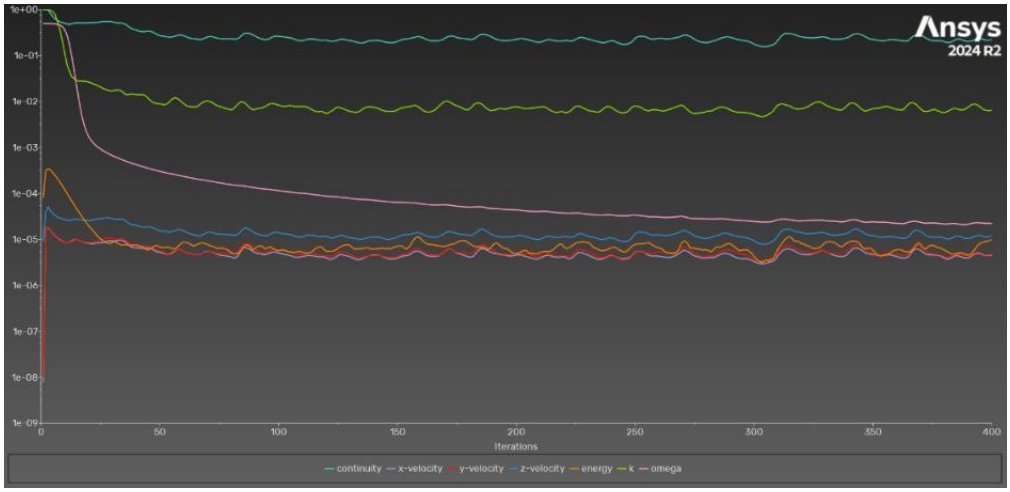



**Figure C-3 Residual history for the A380 cruise case**

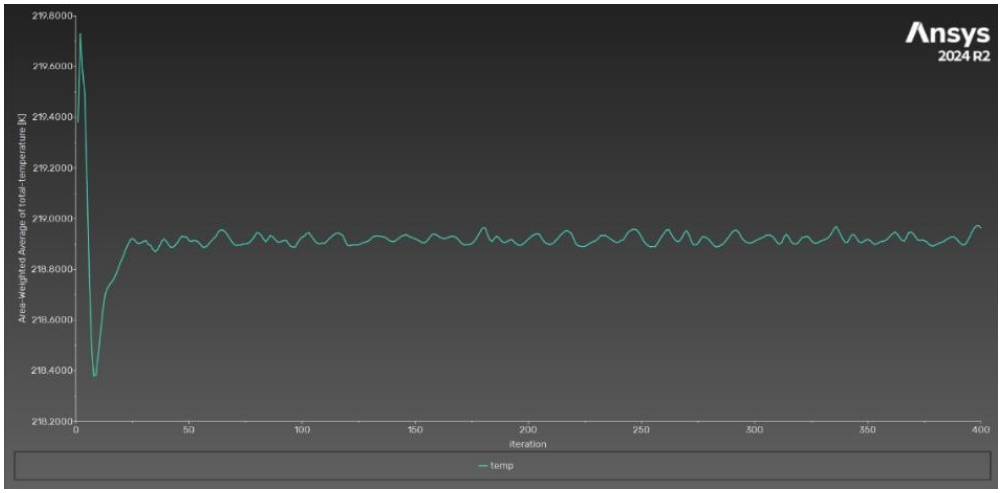



**Figure C-4 Area-weighted average tailplane temperature for the A380 cruise case**

*Multi-phase Conditions for A320:*

- *Taxing*

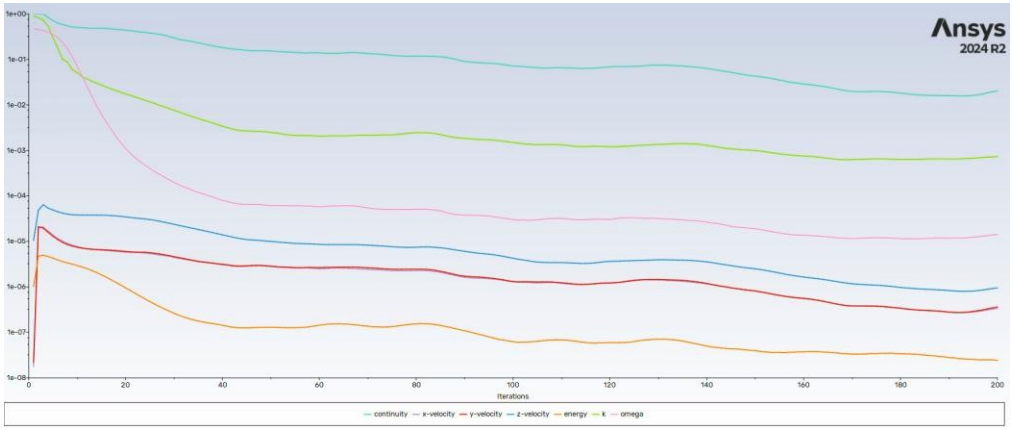



**Figure C-5 Residual history for A320 taxing case**

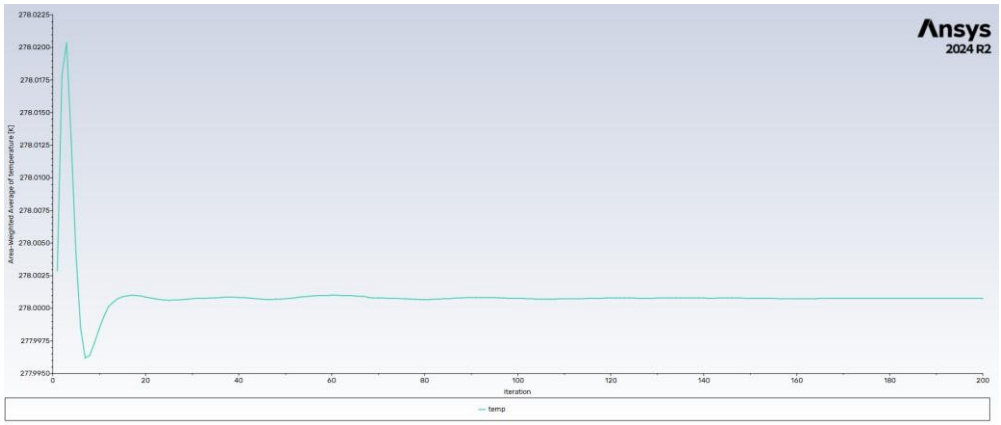



**Figure C-6 Area-weighted average tailplane temperature for the A320 taxing case**

• *Runway*

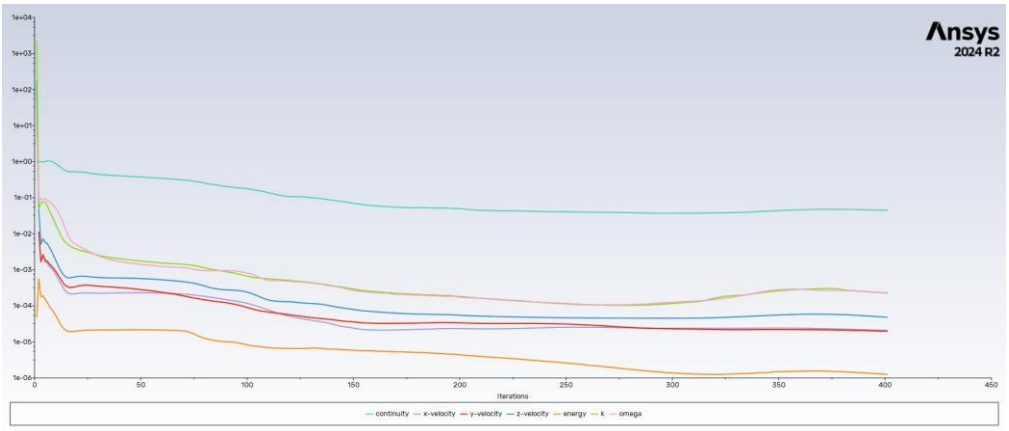



**Figure C-7 Residual history for A320 runway case**

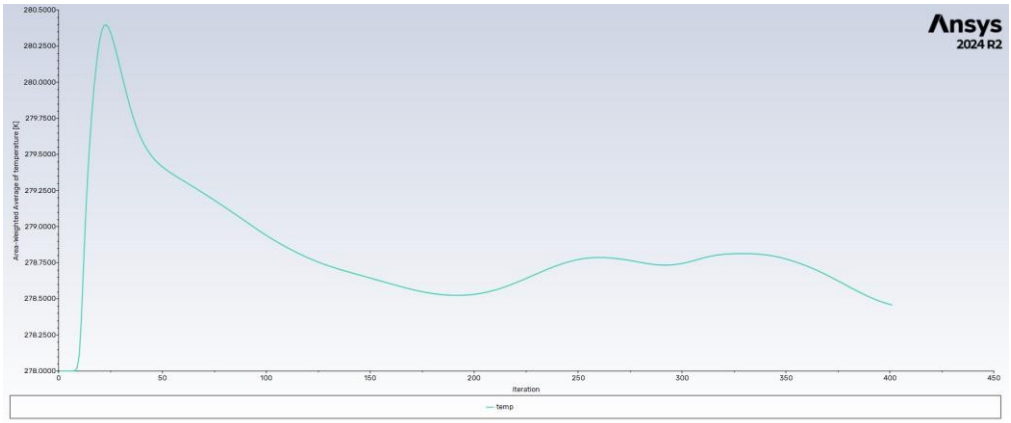



**Figure C-8 Area-weighted average tailplane temperature for the A320 runway case**

• *Cruise*

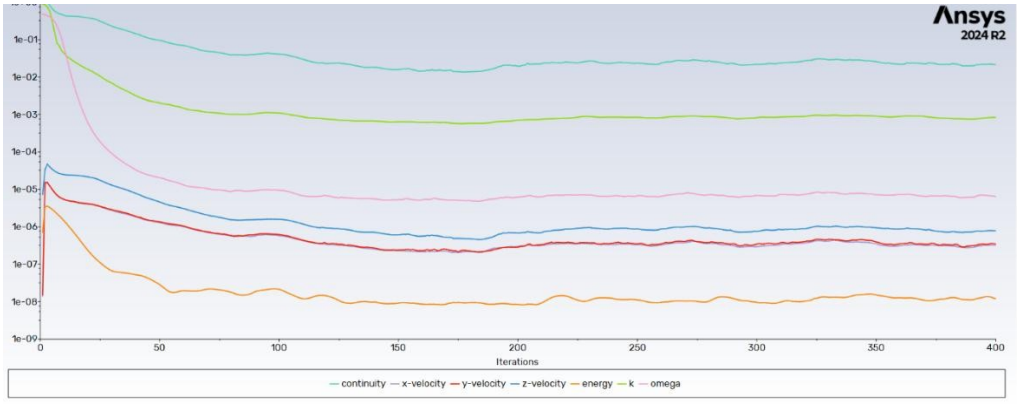



**Figure C-9 Residual history for A320 cruise case**

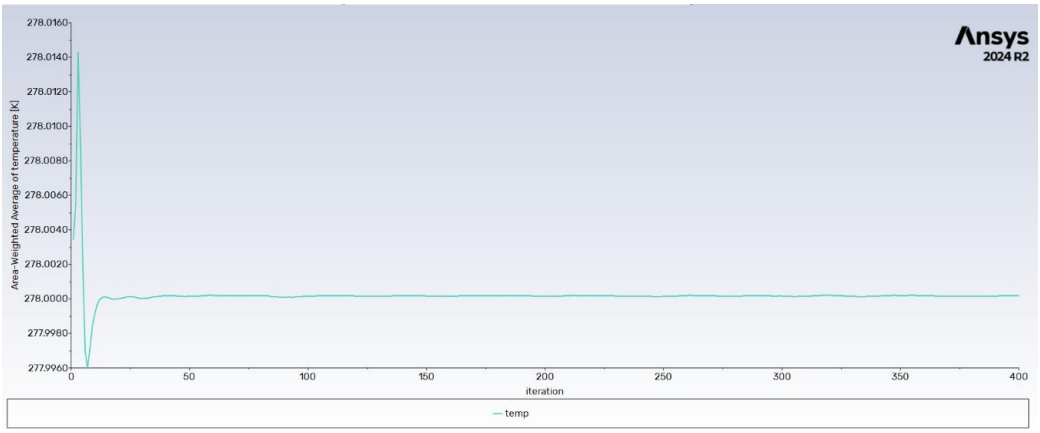



**Figure C-10 Area-weighted average tailplane temperature for the A320 cruise case**

## D. Flow Simulation of Exhaust Plume Interaction with Tailplane

*Cruise Conditions Cases:*

- *A320(CFM56-5B)*

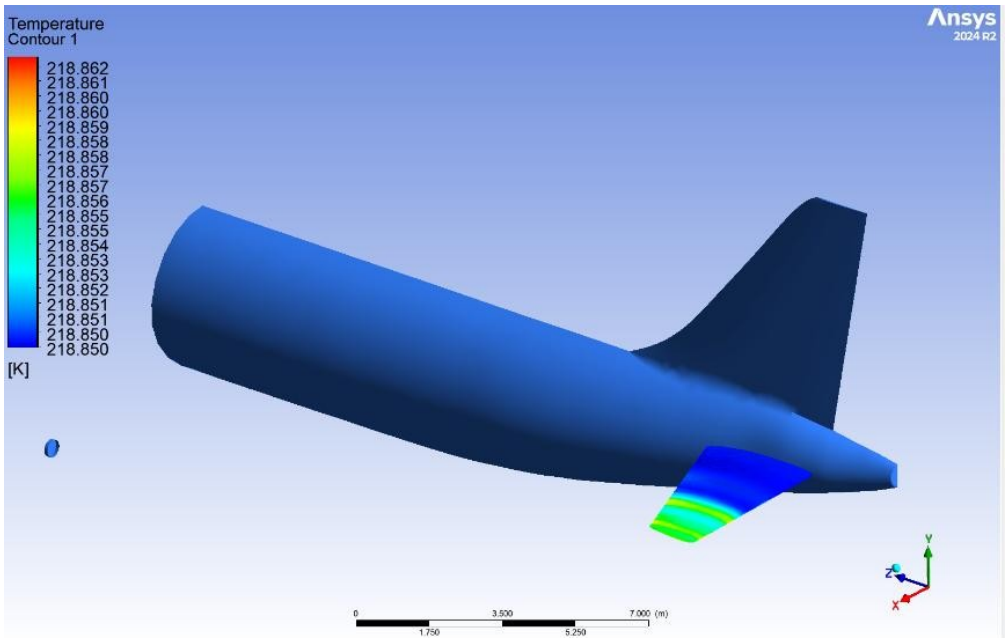



**Figure D-1 Temperature contours of the A320 tailplane during cruise phase (upper rear angle view)**

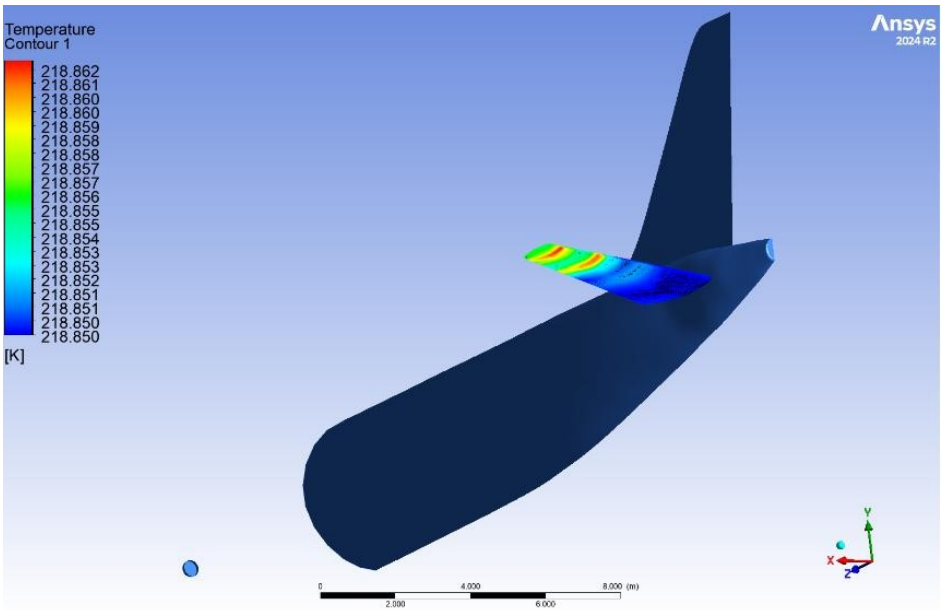



**Figure D-2 Temperature contours of the A320 tailplane during cruise phase (low rear angle view)**

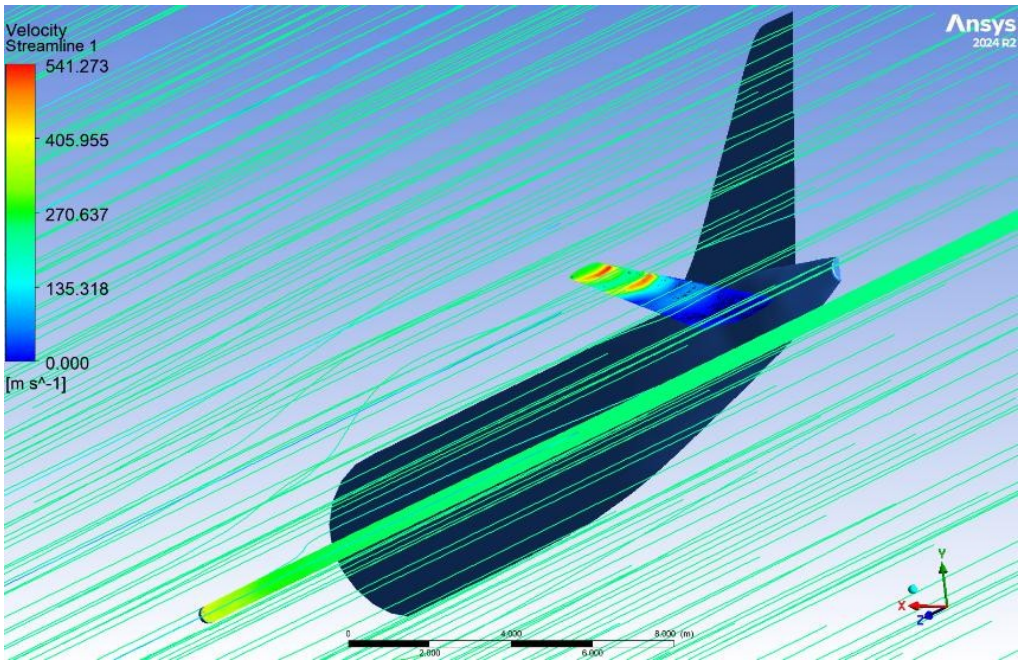



**Figure D-3 A320 cruise case: rear-mounted exhaust plume impinging on tailplane**

- *G280(HTF7250G)*

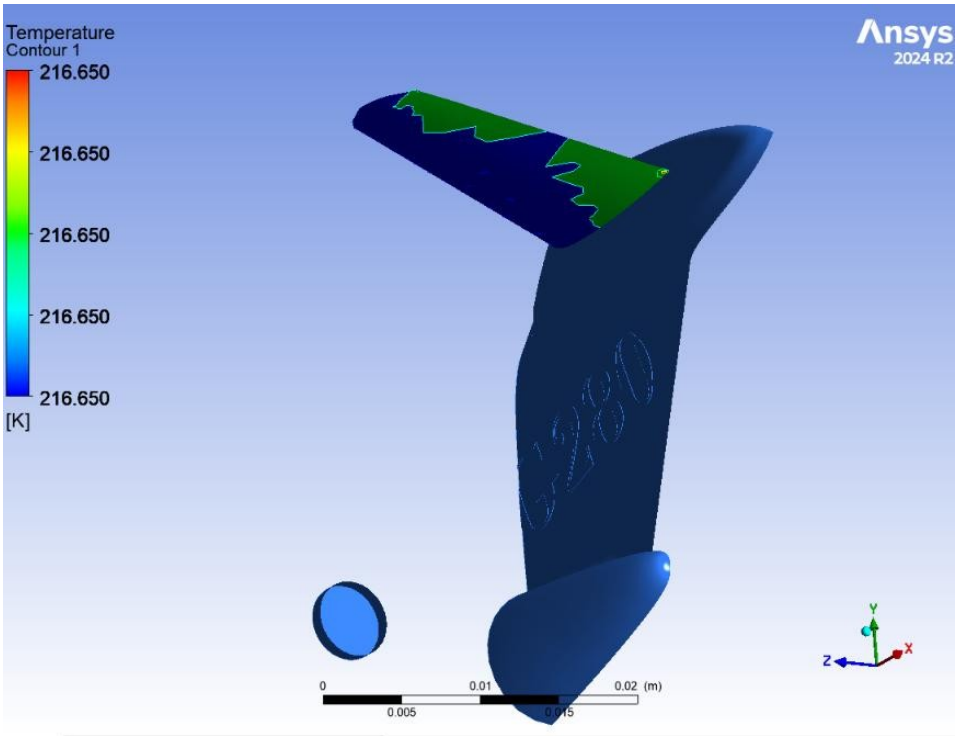



**Figure D-4 Temperature contours of the G280 tailplane during cruise phase (low rear angle view)**

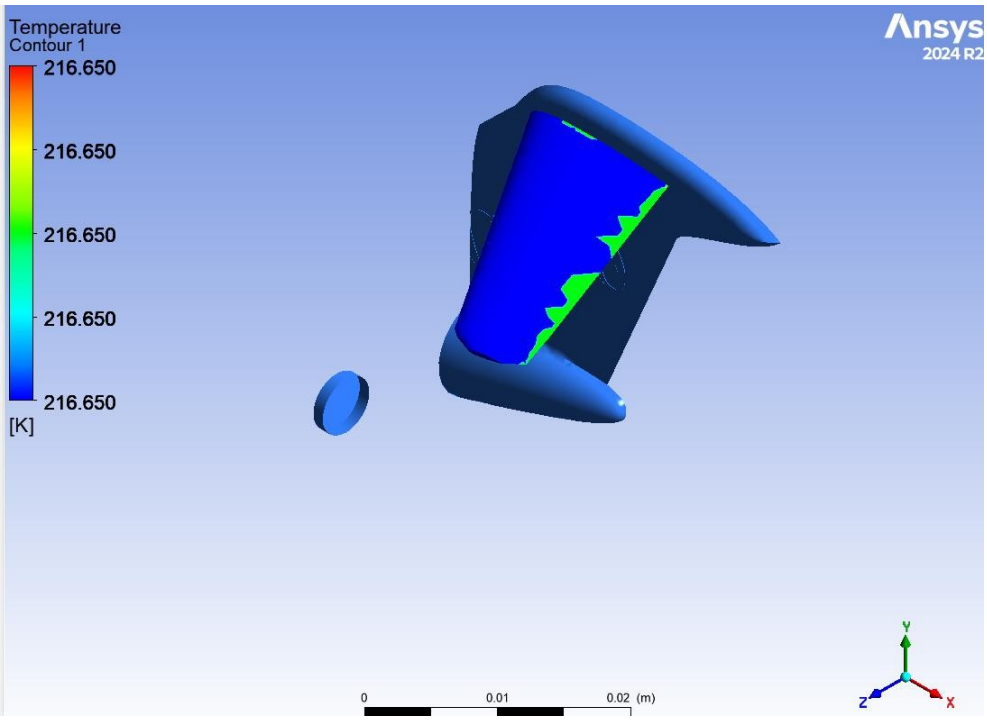



**Figure D-5 Temperature contours of the G280 tailplane during cruise phase (upper rear angle view)**

- *A380(RR Trent 900)*

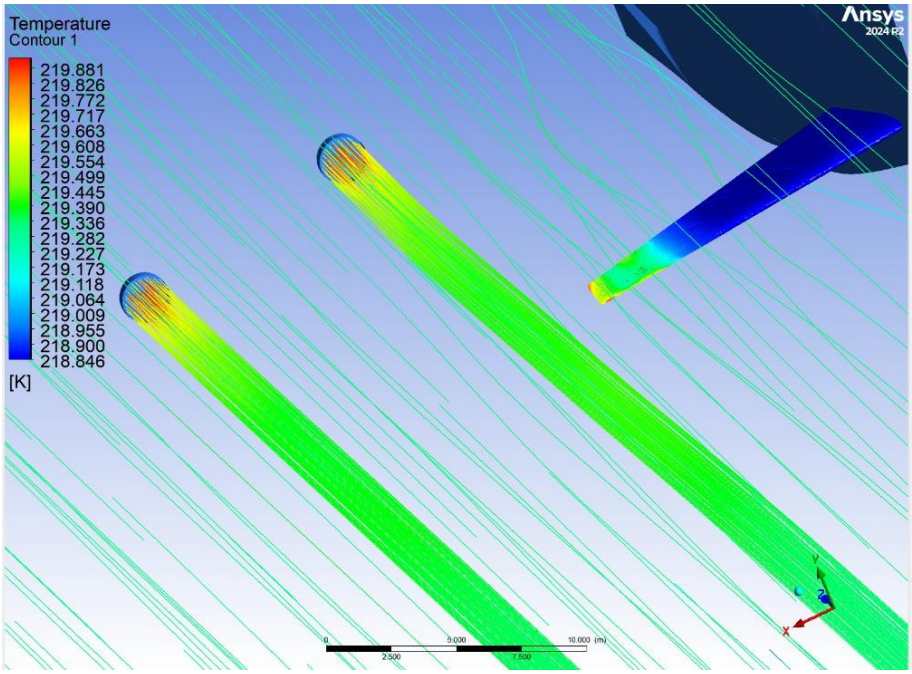



**Figure D-6 A380 cruise case: rear-mounted exhaust plume impinging on tailplane (upper rear angle view)**

*Multi-phase Conditions for A320:*

- *Taxing*

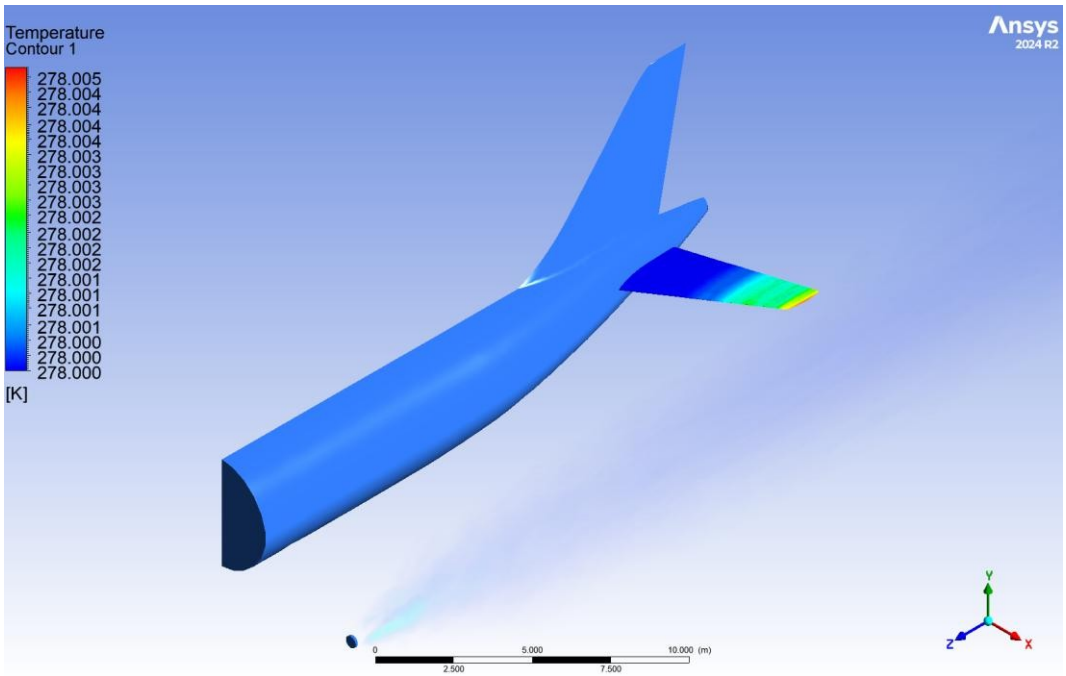



**Figure D-7 Temperature contours of the A320 tailplane during taxing phase**

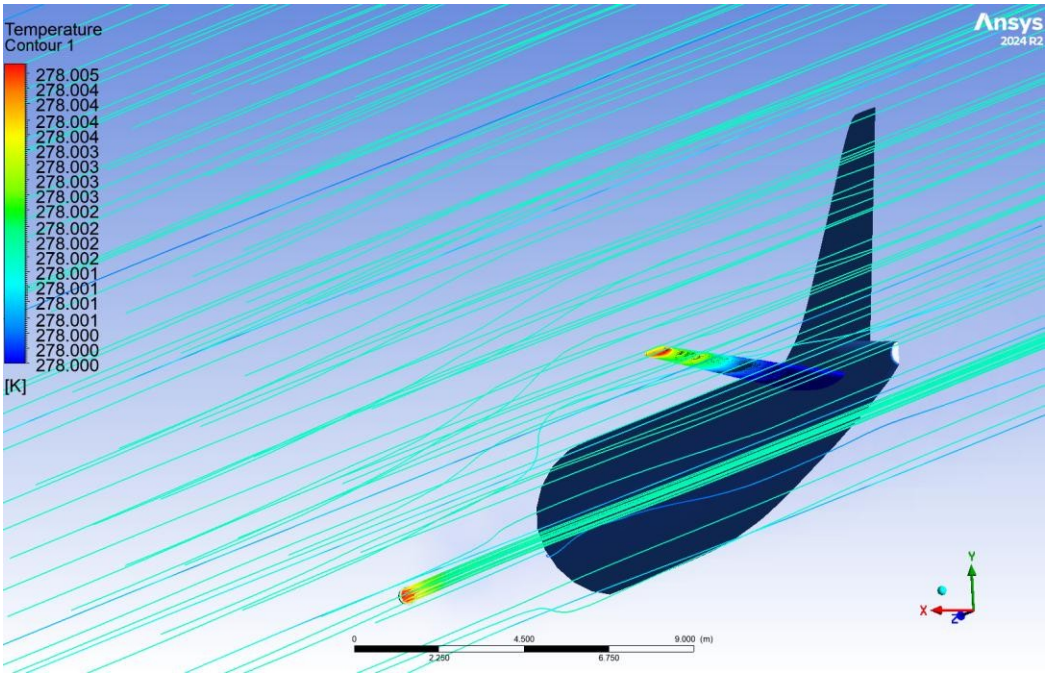



**Figure D-8 Inlet streamlines superimposed with temperature contours during taxing phase(20kts headwind)**

• *Runway*

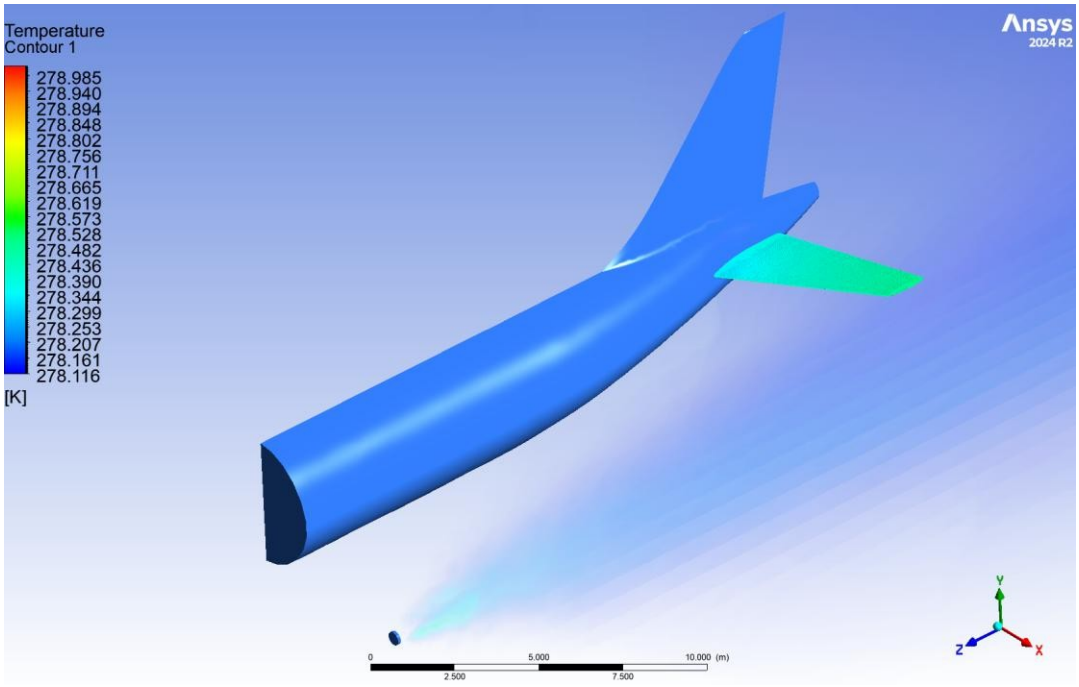



**Figure D-9 Temperature contours of the A320 tailplane during runway phase**

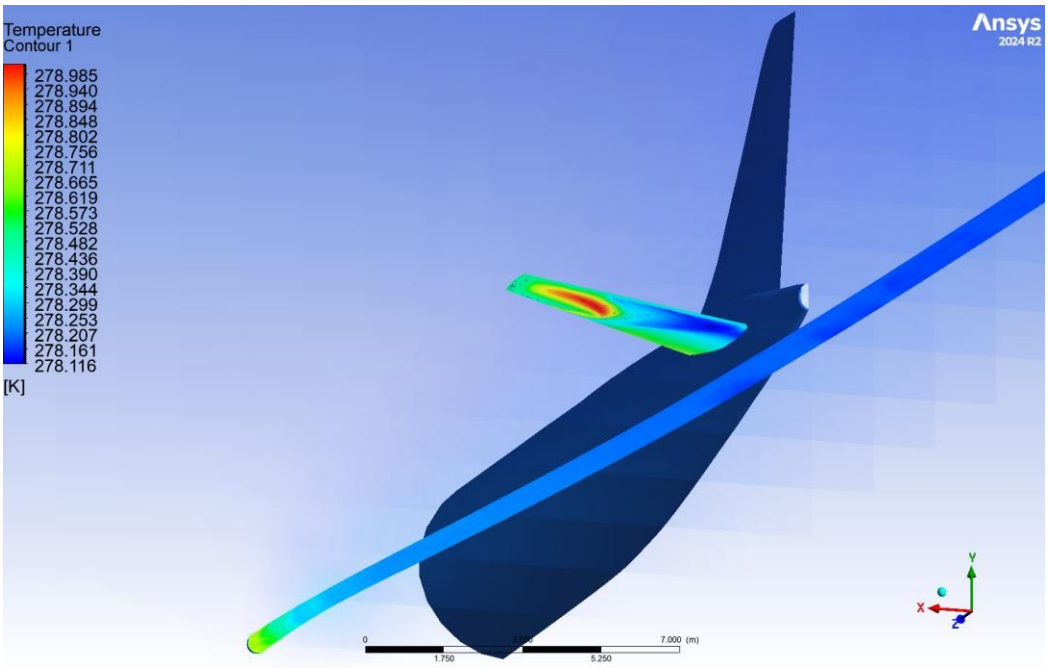



**Figure D-10 A320 runway case: rear-mounted exhaust plumes and impinging on tailplane**

• *Take-Off*

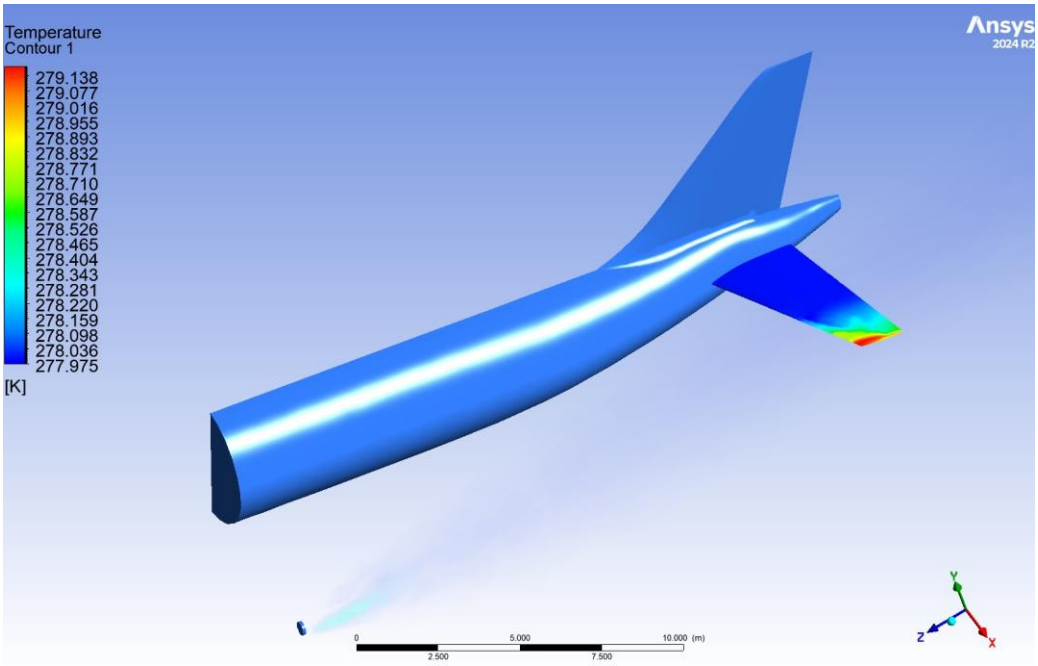



**Figure D-11 Temperature contours of the A320 tailplane during take-off phase**

## E. Thermal Influence on the Tailplane Surface

*Cruise Condition Cases:*

• *A320(CFM56-5B)*

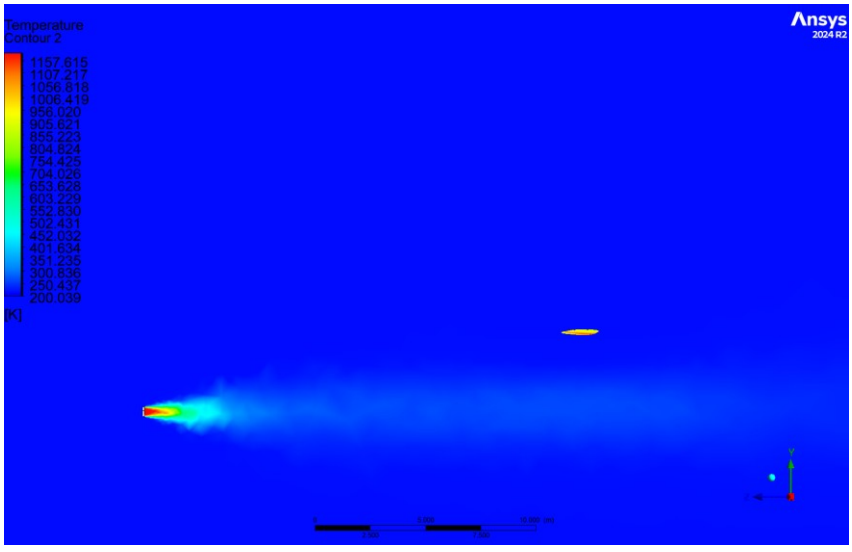



**Figure E-1 Temperature contour of exhaust gases during A320 cruise phase (side view)**

• *G280(HTF7250G)*

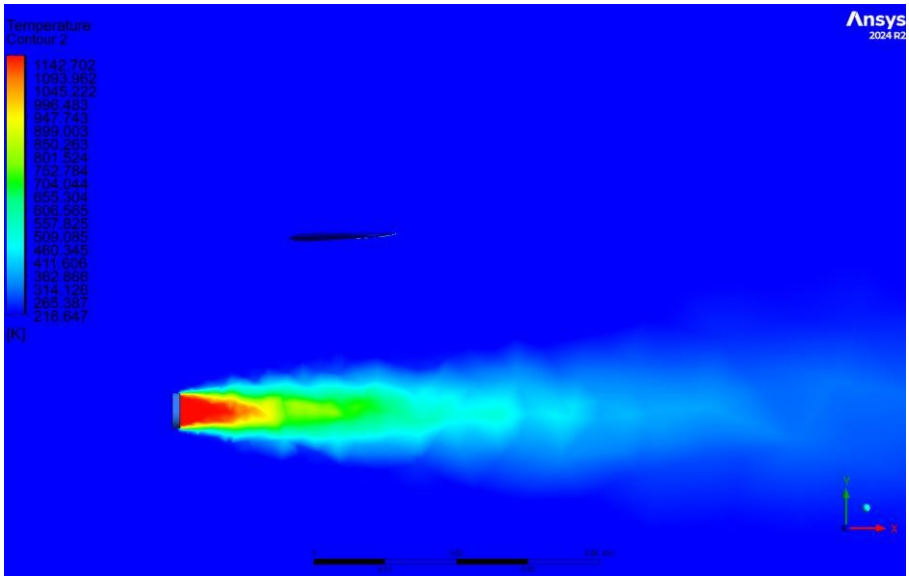



**Figure E-2 Temperature contour of exhaust gases during G280 cruise phase (side view)**

• *A380(RR Trent 900)*

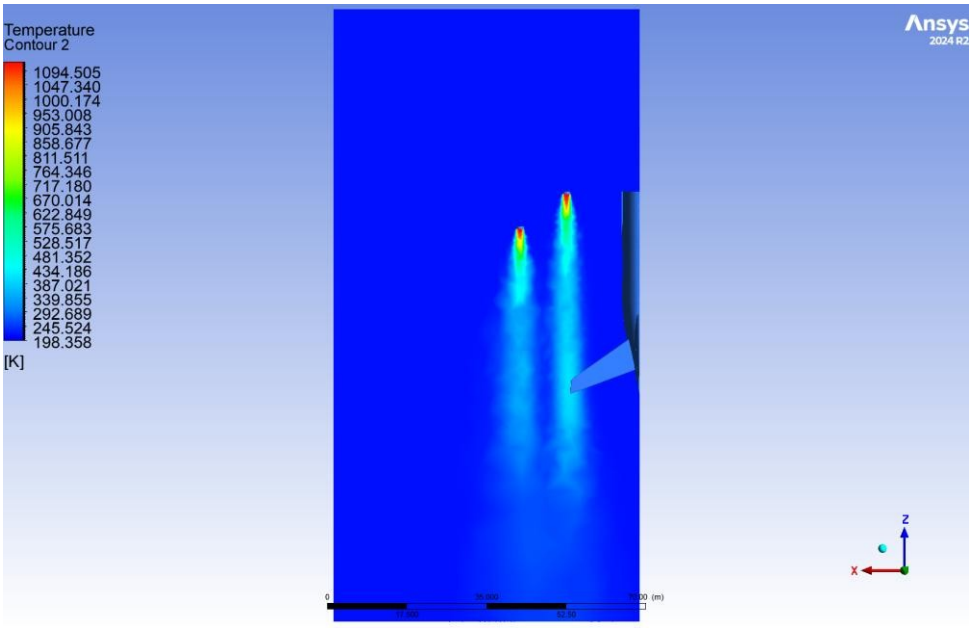



**Figure E-3 Temperature contour of exhaust gases during A380 cruise phase (top view)**

*Multi-phase Conditions for A320:*

- *Taxing*

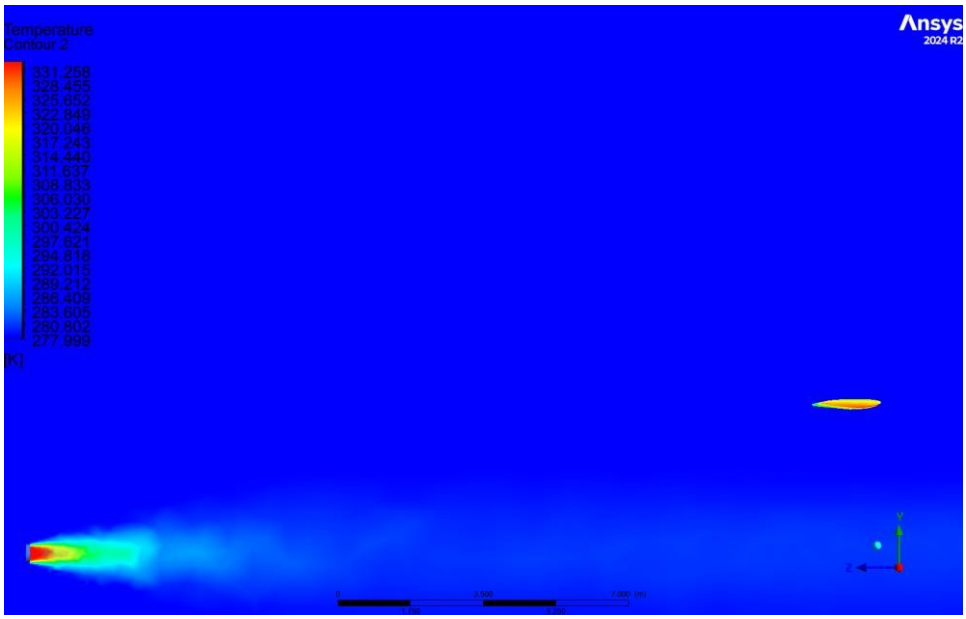



**Figure E-4 Temperature contour of exhaust gases during A320 taxing phase**

- *Runway*

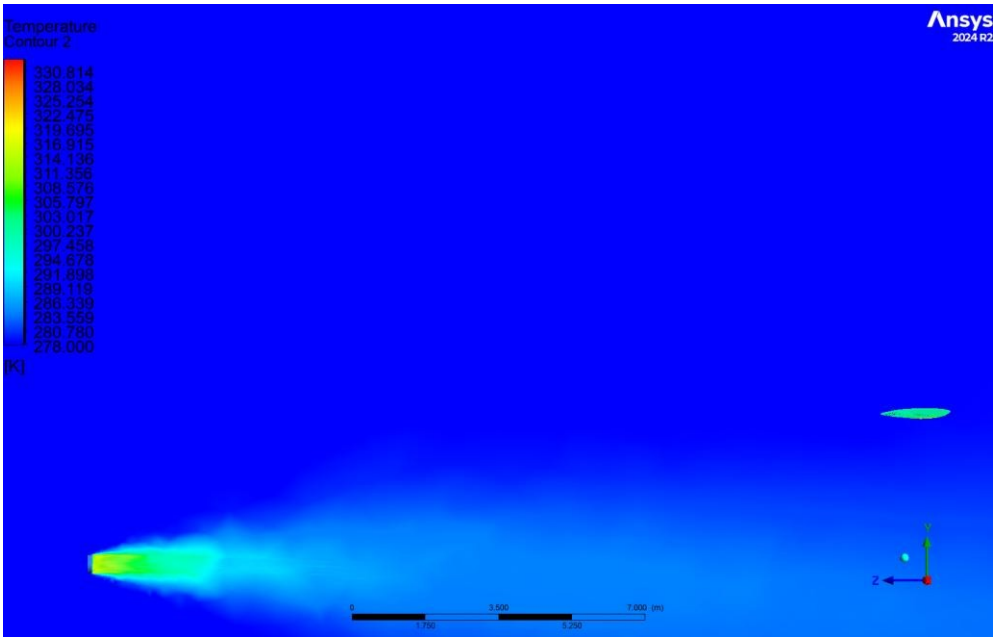



**Figure E-5 Temperature contour of exhaust gases during A320 runway phase**